DELFT UNIVERSITY OF TECHNOLOGY
3ME: PROCESS AND ENERGY
ENERGY TECHNOLOGY

Acoustic coagulation of aerosols

Andries van Wijhe
MSc Thesis
July 2013
Report 2583

Committee:
Prof.dr.ir. B.J. Boersma
Dr.ir. W. de Jong
Dr.ir. P Plaza
Dr.ir. M. Langelaar

LEEGHWATERSTRAAT 44
2628CA DELFT
THE NETHERLANDS

0. Summary

Flue gas from combustion or syngas from gasification can contain fine particles, so called aerosols. These can be potentially harmful for downstream equipment or if emitted to the atmosphere, be inhaled by humans and cause respiratory problems.

Standard practice to mitigate this is to use a cyclone which has a low filtration efficiency for sub-micron sized particles. In the 1920s it has been accidentally discovered that acoustic waves can coagulate aerosols to form bigger sized agglomerates. It has been suggested to use acoustic waves as a pre-treatment step before using a cyclone to increase the filtration efficiency without inducing a pressure or temperature drop on the flow.

A study was done on the possible mechanisms for this coagulation and these are used in a population model based on Smoluchowski's equation. The first mechanism is the orthokinetic particle interaction, which describes a relative velocity of two particles with different entrainment in relation to the velocity field of the acoustic wave. The second mechanism is the acoustic wake effect, an effect in which the distance between particles decreases due to the mutual slipstreaming in an oscillating flow.

To verify if the correct physical relations are identified a lab scale setup was built. An of the shelf piezo-electric transducer intended for under water cleaning was taken apart and put into a FEM model. This model was validated with the use of various measurement methods and concluded was that the FEM model is a good tool to predict the mode shapes and Eigen frequencies, but unable to predict the magnitude of the vibration.

The model was extended with the design of an ultrasonic horn and radiation plate. With these build, sound pressure levels of over 150dB at 41kHz were achieved which are a significant improvement of the transducer without the horn and plate.

Three different experiment series were performed with aerosols of different composition, concentration and particle size. In the first series an aerosol was created by atomizing paraffin oil, which created a visible fog. The treatment of this with an acoustic field resulted in an increase of particle deposition in the coagulation chamber.

In the second experiment series, the aerosol was formed by atomizing a brine solution to form NaCl crystals. The particles coagulated and a shift in the particle size distribution was measured in accordance with the model. The overall coagulation rate is still an uncertainty because of the inability to properly the measure the intensity of the acoustic field inside the chamber.

A final experiment was done with brine atomization, but with helium as a carrier gas which has a lower density than air. As a result the flow rate of the atomizer has to be increased which resulted in a decrease of residence time. Coagulation was measured, but not entirely according to the model predictions.

Concluded was that the model which is based on the orthokinetic particle interaction and the acoustic wake effect is able to predict the coagulation, but in some circumstances it appears that an effect is missing from the model.

Table of Contents

Nomenclature

	Roman	
c	speed of sound	m/s
d	particle diameter/size	m - µm
f	frequency	Hz
l	slip coefficient	
m	(particle) mass	kg
n	bin concentration	particles/m^3
p	pressure	Pa
q	entrainment ratio	
t	time	s
u	particle velocity	m/s
v	sound field velocity	m/s
x	distance	m
	Roman capital	
A	area	m^2
B	isentropic compressibility	Pa^{-1}
CCS	collisional cross section	m^2
D	distance between particles	m
E	collision efficiency	
J	sound intensity	W/m^2
K	coagulation kernel	m^3/s
N	total particle concentration	particles/m^3
Re	Reynolds number	
S	agglomeration efficiency	
U	particle velocity amplitude	m/s
V	sound field velocity amplitude	m/s
Z	acoustic impedance	Ns/m^3
	Greek	
γ	heat capacity ratio	
δ	particle-fluid density ratio	
η_s	isotropic loss factor	
μ	viscosity	Pas
ϕ	volume flow	l/min
θ	angle/phase	rad
ρ	density	kg/m^3
τ	particle relaxation time	s
φ	phase difference	rad
ω	angular frequency	rad/s
	Subscript	
$_p$	particle	
$_f$	fluid	
$_0$	amplitude	
$_r$	reference	
$_{ST}$	Stokes	

1. Introduction

The current energy supply chain is nowadays largely based on combustion and this is not likely to change in the near future. Even though a transition from fossil to renewable energy is forthcoming, the cheapest form of renewable energy in the Netherlands is the co-firing of biomass at coal fired power plants.

Biomass is a very versatile fuel which is available throughout the world, but it also a very difficult fuel. Its varying composition can cause problems concerning dust emission due to high alkali, chlorine and ash contents of some fuels[4]. If the biomass is combusted, these are partly emitted as aerosols in the flue gas stream, if a gasification process is used, these can be released in the syngas produced.

Aerosols are nothing more than fine suspended solid particles or liquid droplets in a gaseous medium. These can be quite useful for example in deodorant or spray paint. However, aerosols are also released in the combustion or gasification of hydrocarbons and can be, depending on the application, released in the atmosphere or carried on to downstream equipment.

The combustion of biomass can lead to very high emission of submicron and supermicron particles in the flue gas stream with concentrations that can vastly exceed 50mg/m^3[4]. This matter consists of particles which can result from incomplete combustion such as soot, tar and inorganic materials from the fuel ash such as silica or inorganic salts

PM10 particles (particles with a size up to 10µm) are known to cause an increase in asthma and COPD for susceptible persons and can cause deaths due to heart attacks, stokes or respiratory causes[5]. Submicron sized particle can deposit very deep in the alveolar region of the lungs[6, 7] and experiments with ultrafine particles (<100nm) of carbon black and TiO_2 show that they have a greater inflammatory effects than bigger particles with the same dose. The mechanism of this nanotoxicity is not yet fully understood but the high surface area of the ultrafine particles seem to be of importance[5, 8]. Another effect of particles in smaller size ranges is that physical properties such as color and solubility of the material can change at ultrafine scales [9].

Downstream equipment of gasification or combustion can be harmed by aerosol emission. For instance inorganic salt particles can poison or foul SCR catalysts for the reduction of harmful NO_x emission[10] which is accelerated by the use of biomass[11]. For the promising combination of biomass gasification and solid oxide fuel cells for power generation, the deposition of tars can affect the operation of the anodes of the fuel cells[12].

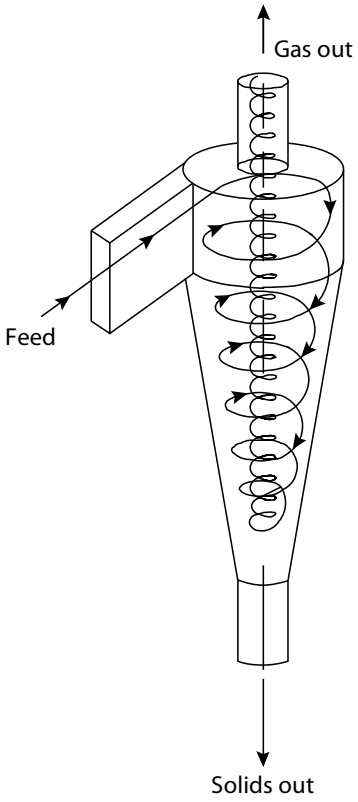

Figure 1-1 Reverse-flow cyclone [3]

1.1. Aerosol filtration (current techniques and their drawbacks)

Current filter technologies are not always sufficient to remove small size aerosols from gas streams. A filter such as a baghouse is an effective means of removing aerosols, but is limited to an operating temperature of around 250°C[13]. Ceramic filter candles offer a much higher temperature resistance, a reasonable pressure drop and the possibility of adding an internal catalyst for internal gas processing[13] but require regular cleaning with nitrogen pulses[14] and this is expensive[15].

Wet separation such as washing can remove particles down to 0.5µm, spray towers have a low pressure drop, but cannot remove particles below 10µm[3]. The disadvantage of wet separation is a significant temperature reduction which makes the use of a downstream SCR infeasible because of the higher temperatures involved.

Another method of separating aerosols from a gas stream is by using a cyclone. The shape of the cyclone (FIGURE 1-1) causes a vortex in which centrifugal forces move the particles to the wall. At the bottom, the particles drop down due to the gravity and the air stream moves through the core of the vortex which has a lower pressure and leave the cyclone at the top. Cyclones are inexpensive, have a low pressure drop (500-1500Pa)[16] and their operating principle is very well understood[3, 16]. However they are not very good at removing fine particles[17].

Another option for aerosol removal is an electrostatic precipitator which uses high voltage electrodes to ionize the passing gas, charging the particles. The particles then are attracted to the electrodes where they stick and need to be removed by another mechanism. Electrostatic precipitators have a high particle removal efficiency even at fine particle sizes, but are bulky and expensive to acquire and operate[3, 18].

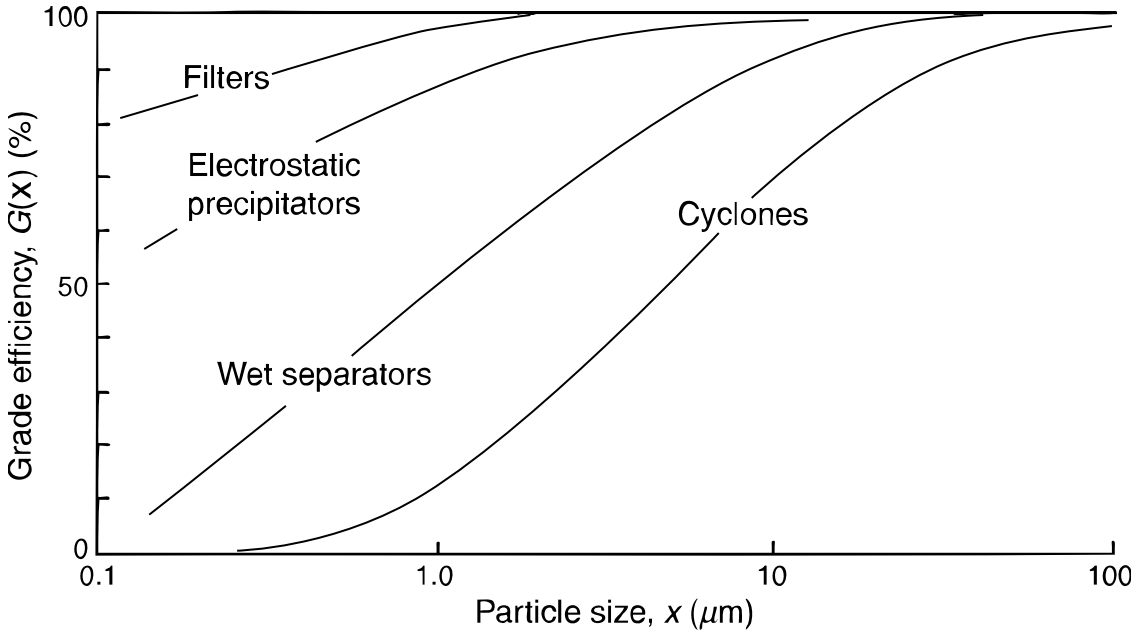

Figure 1-2: Filtration efficiency of common technologies[16]

1.2. Acoustic coagulation of aerosols

This thesis discusses a method of coagulating fine particles by using a high intensity ultrasonic sound field. The consequence of the coagulation is a shift in the particle size distribution (PSD) to a bigger

particle size. In case fine particles have to be removed from a gas stream for which the temperature is too high for fabric-based filtration and the gas should not cool down, the only two options would be a candle filter or an electrostatic precipitator which are both expensive and the latter is bulky. An alternative would be a cascade of an coagulation chamber and a cyclone for which the possibilities will be discussed in this work.

1.3. Scientific history relating to the acoustic coagulation of aerosols

One of the first relevant physical experiments was done by Dr. August Kundt almost 150 years ago. He build an apparatus to measure the speed of sound by creating a standing wave with a moving piston inside a cylinder[19]. Inside he tube he put some fine powder such as cork particles. The powder settles in higher concentrations at the antinodes and by measuring the distance (x) and the frequency known, the speed of sound can be calculated:

$$c = 2xf \tag{1.1}$$

Paul Langevin pioneered in the field of macrosonics in 1917, which is the part of acoustics related to high intensity sound waves, by using a quartz ultrasonic transducer which were used for submarine sonar systems[7].

In 1926 prof. R.W. Wood and A.L. Loomis performed some experiments on the physical effects in liquid media of high power acoustics with frequencies in the hundreds of kilohertz region [7, 20-22]. In 1929 C. Andrade and S.K. Lewer noticed the ring shaped deposition of dust particles in the antinodes of a sound wave in a tube[23]. H.S. Patterson and W. Cawood performed experiments with a an ultrasonic wave in a smoke filled cylindrical tube and noticed not only the depositions, but also the appearance of agglomerates[24]. They did the experiments in 1927, but published it 4 years later.

In the 1960s a lot of research was done by Soviet scientists on acoustic coagulation of aerosols, one of their intended functions for it was to clear airstrip runways from fog with the use of powerful sirens[22]. The fundamental mechanics of acoustic coagulation of aerosols was also extensively researched in the Soviet Union, and literature from that period is still very relevant. The book *The mechanics of aerosols* from N.A. Fuchs[21] published in English in 1964 is a good starting point for any research relating to aerosols. The book *Acoustic coagulation and precipitation of aerosols* from E.P. Mednikov[22] is even more applied to the subject and it is hard to find a paper in this subject without this in the reference list. It offers an extensive review of all the theoretical and practical implications of aerosol treatment with an acoustic field.

The scientists in the Soviet Union used whistles and sirens for their experiments which can achieve high sound pressure levels, but offer low efficiency. In the end of the 1970s J.A. Gallego-Juarez invented an ultrasonic transducer based on the 'Langevin Tonpilz' used previously on submarines. This invention offers high sound pressure levels (SPL) at the desired efficiency[25]. A selection of more recent experiments can be found in Table 1-1.

Since the 1980s the modeling of the discussed process gained interest by a few scientists such as S. Temkin and T.L. Hoffmann. They used the Smoluchkowski model for Brownian coagulation and adapted it to be used for acoustic coagulation. The nature of this modeling requires also an amount of computational power which was not available in the 1960s.

Table 1-1: A selection of similar experiments since the 1970s

Year	Author	Aerosol type	ultrasound	Result
1975	Scott[26]	ZnO fume	15kHz 160-165dB pulse-jet τ=2-5s	A PSD shift showing a decrease in the ~1µm and an increase in the ~3-7µm region, cyclone collection efficiency increased from 30-40% to 40-80%
1979	Shaw et al. [27]	0.085/0.5/1.0µm Polystrene latex spheres $50/4.7/1.7 \cdot 10^{10}$ p/cm^3 0.12/0.17µm dioctyl phthalate vapor $60\text{-}70 \cdot 10^{10}$ p/m^3	1-3kHz electromagnetic speaker 10kHz siren 145dB	The theoretical (Brownian and orthokinetic) coagulation kernel constant is underestimating the measurements in the region ~0.1µm, in the 1µm size range the measurements show a spread of almost a factor 1000.
1986	Riera-Franco et al.[28]	0.2-0.9µm Poly-disperse carbon black, 4.5-9.1 g/m^3	20.4khz 156-163dB piezo transducer with stepped plate τ=1-5s	The dynamic growth index was defined as the ratio of the particles ratio before and after treatment, measured values are
1987	Tiwary et al.[29]	5µm coal fly-ash 1-30g/m^3	1.4-2.5kHz siren 140-160dB τ=2-6s	Rapid increase of particle size to 10µm with t=2-4s and a SPL of 160dB.
1991	Somers et al.[30]	Glycol drops 10-1000 $\cdot 10^{10}$ p/cm^3 ~1µm TiO_2 particles 10-$200 \cdot 10^{10}$ p/cm^3 τ=60-300s	21kHz	Decrease of particle concentration: 0.5-3.5 orders of magnitude for glycol fog, +/- 1 order of magnitude for TiO_2.
1999	Gallego-Juárez et al.[31]	fluidized bed coal combustor 0.1/1µm/20µm 1-5g/m^3 2000m^3/h τ=2/3s	2/4 units 10/20kHz piezo transducers with stepped plate 80/400W	Reduction of submicron and supermicron particles of up to ~40% in an actual application in combination with an ESP.
2012	Buntsma [32]	cigarette smoke (See: paragraph 4.2)	28kHz piezo transducer ~150dB 120W	Visible clues that ultrasound treatment enhances coagulation of aerosols.

1.4. Research questions

It is stated that acoustic coagulation of aerosols is a potential enhancement in removing aerosols from gas streams, but the effectiveness of the process still needs to be evaluated to suggest an actual implementation. This means that driving forces behind the coagulation should be well understood. To evaluate the application potential of this technology the main research question is:

What are the mechanisms of acoustic coagulation of aerosols?

This can be divided into four sub questions:

- *Which physical effects are of major influence on acoustic coagulation?*

- *How do the properties of the gas and the aerosols influence the process?*
- *What is the influence of sound pressure level and residence time?*
- *Can a population based model be validated by a low cost small scale setup?*

1.5. Hypothesis

- Aerosols treated with high intensity ultrasound irradiation undergo extensive coagulation due to their difference in motion relative to the sound wave and their mutual wake interaction. This effect will cause a shift in the particle size distribution, which can be predicted using a population balance (Smoluchkowski equation) and measured by methods of optical scattering.

1.6. Methods

The hypothesis will be tested by a mathematical model which is based on the Smoluchowski equation. Also a lab scale setup will be built to evaluate the results of the model. The ultrasonic radiation source will be constructed from an of the shelf transducer for ultrasonic cleaning with an extension to better match the acoustic impedance of air.

Chapter 2 will discuss the relevant physical phenomena and give a description of the model. Chapter 3 will elaborate on the design and test of the ultrasonic transducer. Chapter 4 will give a general description of the small scale test setup for acoustic coagulation of aerosols, followed by the results in chapter 5 and a conclusion in chapter 6.

2. Theoretical background on acoustic coagulation

2.1. Acoustics

The mathematical description of a sound wave can be derived from the equation of motion for an elastic rod, for which the differential equation of movement is [33]:

$$\frac{\partial^2 u(x,t)}{\partial t^2} = \frac{k_l}{m_l}\frac{\partial^2 u(x,t)}{\partial x^2} \tag{2.1}$$

In which the subscript *l* relates to the fact that the properties are per length unit. For a column of air, a similar equation can be set up. The mass per length of an air column is: $m_l = \rho A$ and the stiffness is $k_l = BA$.

$$\frac{\partial^2 v(x,t)}{\partial t^2} = \frac{B}{\rho}\frac{\partial^2 v(x,t)}{\partial x^2} \tag{2.2}$$

The isotropic compressibility of the air B can be defined using the ideal gas law under adiabatic conditions:

$$B = \gamma p \tag{2.3}$$

By using equation (2.3) and solving differential equation(2.2), the wave velocity of a moving sound wave is derived:

$$c = \sqrt{\frac{p}{\rho}\gamma} \tag{2.4}$$

One other important aspect of acoustics for this research is the acoustic impedance. Simply put it is the ratio between the velocity of the movement of the medium in the sound wave and the pressure variations. Sound intensity is expressed in sound pressure level (SPL) while the velocity of the medium is important for the coagulation. A detailed explanation of the relation between the movement of molecules and its pressure can be found at appendix B.

2.1.1. Non-linear acoustics

In equation (2.4) the propagation velocity of acoustic waves is defined as dependent on the pressure, this means that the high pressure region of the wave moves faster than the low pressure region. The result of this is a deformation of the sound wave. Because part of the wave travels faster than other parts, the sine shaped wave of the sound transforms to something that resembles a saw-tooth[7, 22], which means that higher harmonics are super-positioned on the original wave. Many of the proposed coagulation effects are based non-linear acoustics[17].

2.2. General equation of particle motion

Aerosols can be modeled by setting up a differential equation for describing the motion of individual particles, assuming that the particle only undergoes a drag force:

$$\frac{du}{dt} = \frac{F_{drag}(u,v)}{m} \tag{2.5}$$

Note that u is the velocity of the particle and v is the velocity of the surrounding gas.

2.2.1. Drag force

The Reynolds number is defined as the ratio between the inertial forces and the viscous forces, it is defined for spherical particles as:

$$\mathrm{Re}_d \equiv \frac{\rho_f \left(u - v\right) d}{\mu} \tag{2.6}$$

This means that fine particles will be influenced more by forces due to viscosity than due to inertia. With the inertia neglected, the Navier-Stokes equation reduces to[34]:

$$0 = \nabla p + \mu \nabla^2 v \tag{2.7}$$

This is called Stokes flow after Sir George Gabriel Stokes. With this equation, the drag force of a static spherical particle in a steady flow can be derived. The resulting drag force consists of one third of pressure drag force and two thirds of skin friction due to viscosity[34, 35] :

$$F_{drag} = 3\pi\mu\left(u - v\right) d \tag{2.8}$$

The velocity field around the particle can be described by the following equations in a spherical coordinate system[35]:

$$\begin{aligned} u_r &= 2u\cos\theta\left(\frac{3}{8}\frac{d}{D} - \frac{1}{24}\frac{d^3}{D^3}\right) \\ u_\theta &= -u\sin\theta\left(\frac{3}{8}\frac{d}{D} - \frac{1}{24}\frac{d^3}{D^3}\right) \end{aligned} \tag{2.9}$$

The problem with this approximation is that the stokes flow field is symmetric, also evaluating the inertial term of the Navier-Stokes equation in the Stokes solution shows that this term is not negligible at larger distances from the particle. The Swedish physicist Carl Wilhelm Oseen added a linearized convective term to the Stokes approach[36] and a higher order solution was added by Chester and Breach[37] These equations and more complex approaches can be found in Appendix A.

2.3. Orthokinetic particle interaction

Assuming sinusoidal movement of the air and the particles, the movement equations for both are assumed to have the following solution:

$$\begin{aligned} u &= U\sin\left(\omega t + \varphi\right) \\ v &= V\sin\left(\omega t + \theta\right) \end{aligned} \tag{2.10}$$

This means that the movement of the particles regarding to the movement of the gas medium around it can be characterized as an entrainment ratio and a phase difference:

$$\begin{aligned} q &\equiv \frac{U}{V} \\ &\tan\left(\varphi - \theta\right) \end{aligned} \tag{2.11}$$

The entrainment ratio and phase difference depend on the physical properties of the gas and aerosol. In the most simple approach, the entrainment ratio depends is calculated from the Stokes flow assumption. This means that two particles with a different size experience a relative velocity to each other. This is referred to as the orthokinetic particle interaction and is likely to be the main driving force for aerosol coagulation under the influence of acoustic waves[22, 38].

2.3.1. BFH entrainment ratio

A mathematic description for the entrainment ratio was first described by W. König as early as 1891 for which a detailed derivation can be found at Appendix A. A more simple solution was presented by Brandt, Freund and Hiedemann in 1936[39], in which they took the stokes force for spherical particles as the only influence of particle entrainment ratio and solved the differential equation which is a combination of equation (2.5), (2.8) and (2.10)[22]:

$$\begin{aligned} m\frac{du}{dt} &= \frac{1}{6}\pi d^3\rho_p\frac{du}{dt} = 3\pi\mu_g d\left(v-u\right) \\ \frac{d^2\rho_p}{18\mu_g}\frac{du}{dt} &+ u = v \end{aligned} \tag{2.12}$$

The equation can be simplified by introducing a constant, the particle relaxation time, which is an important factor in aerosol dynamics[21, 22]:

$$\tau \equiv \frac{d^2\rho_p}{18\mu_g} \tag{2.13}$$

Solving the ordinary differential equations yields the following solution:

$$u = \frac{V}{\sqrt{1+\omega^2\tau^2}}\sin\left(\omega t-\varphi\right) + \underbrace{\frac{\omega\tau V}{1+\omega^2\tau^2}e^{-\frac{t}{\tau}}}_{\to 0} \tag{2.14}$$

So the entrainment ratio and phase difference is:

$$q = \frac{1}{\sqrt{1+\omega^2\tau^2}} \tag{2.15}$$

$$\tan\left(\varphi-\theta\right) = \omega\tau \tag{2.16}$$

The difference of particle size on the ratio of entrainment between gas and particle is visible in Figure 2-2 (which is according to the BFH entrainment ratio) and Figure 2-1 (physical evidence of difference in entrainment ratio.).

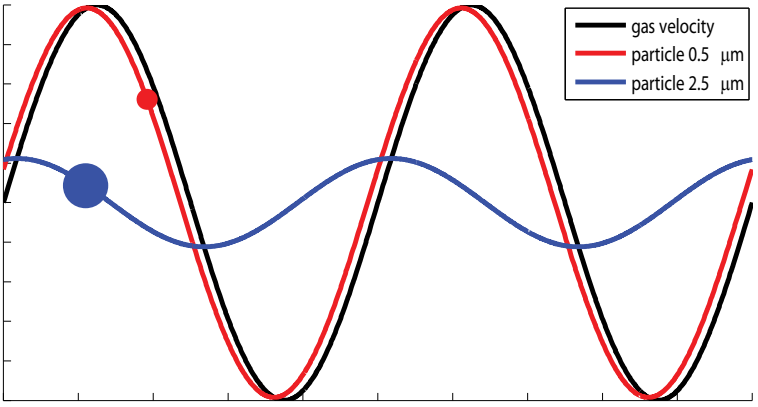

Figure 2-2: Difference of entrainment ratio for two particles of a different size.

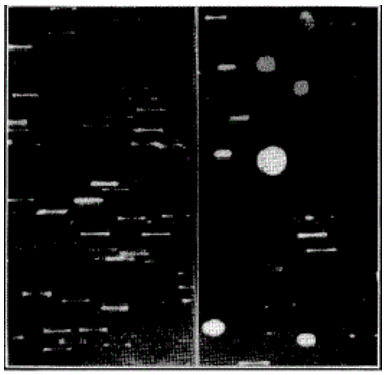

Figure 2-1: Difference in entrainment ratio, left: small particles, right: larger particles[2]

2.3.2. Other entrainment ratio concepts

An expression for the entrainment ratio based on Oseen's approximation was derived by A. S. Denisov in 1965[40]. S. Temkin derived an entrainment ratio based on the Basset-Boussinesq-Oseen equation in 1981[41]. These are discussed in Appendix A.

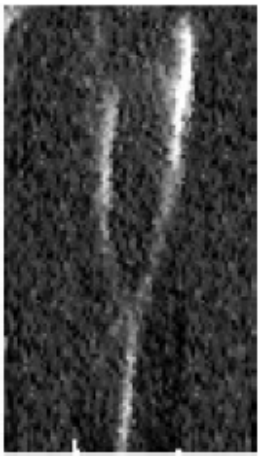

Figure 2-4: Two particles (~8µm) entrained in a horizontal acoustic field and vertical gravity, the particles have the same size and have an initial particle separation of around 140-150µm and collide within 20ms at 5kHz, V=0.44 m/s, Re=0.23 [1]

2.4. *Acoustic wake effect*

The orthokinetic particle interaction describes a parallel motion for two particles with the same size. Because of this, the two particles would not be able to collide. Practical experiments have shown that two particles with the same size do attract under the influence of acoustic waves[1]. In this particular experiment, 2 particles are photographed while undergoing gravity in the vertical direction and an acoustic radiation in the horizontal direction. The resulting picture is defined as the 'tuning fork' for evident reasons and show clear agglomeration.

The effect, first noted by Andrade[21, 42], is caused by a bilateral distortion of the flow field behind the particle and is mentioned by Mednikov as the parakinetic interaction between aerosols[22] but is referred to as the acoustic wake effect in more modern literature[41, 43].

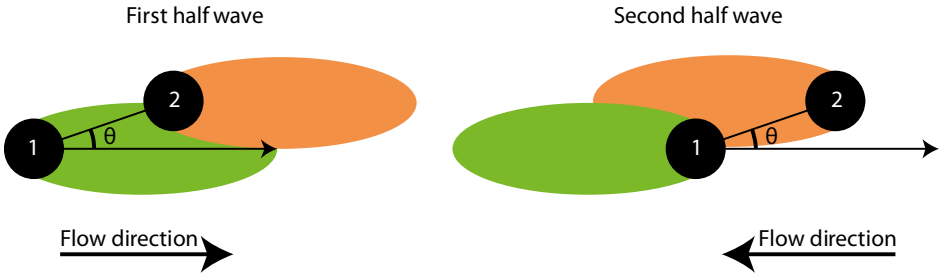

Figure 2-3: The acoustic wake effect

The effect is illustrated in Figure 2-3, in the first half wave particle 2 has a decreased drag due to the wake of particle 1, therefor increasing in velocity. When the sound wave reverses, particle 1 has a decreased drag force due to particle 2 and increases in velocity. Both effects lead to a decrease in distance between particle 1 and 2.

The derivation of mathematical equations describing this effect is rather challenging. An obvious method is to use the velocity field described in equation (2.9) and apply it to the particle which is currently 'behind' the other particle in the current flow field.

The Stokes equation is not suitable for this[34], and will lead to a result which is inaccurate if the distance between the particles is in a higher order of magnitude as the particle diameter[44]. The reason for this is that the Stokes force assumes symmetry in the flow field which is not the case. The Oseen's approximation is an improvement especially for large distances from the particle. According to Oseen's solution the medium velocity decreases with $1/r^2$ in front of the particle and with a rate $1/r$ behind the sphere[45].

The problem was worked out for particle wake interaction based on Oseen's flow by D.B. Dianov in a paper from 1968 in which he derived the time averaged velocity between two particles due to the acoustic wake effect and came to a remarkably easy solution[1, 46]:

$$u_{ij} = \frac{3}{4}\frac{V}{\pi D}\left(d_i l_i + d_j l_j\right) \tag{2.17}$$

With the slip coefficient (This is what Mednikov calls the flow-around factor) in the Oseen's regime which in turn is derived from the slip coefficient in the Stokes regime[41, 46]:

$$l_i = \frac{l_{ST,i}}{\sqrt{1 + 2h_i l_{ST,i}^2 + h_i^2 l_{ST,i}^4}} \qquad \begin{matrix} h_i = \dfrac{9V}{\pi\omega d_i}\dfrac{\rho_f}{\rho_p} \\ l_{i,ST} = \dfrac{\omega\tau_i}{\sqrt{1+\omega^2\tau_i^2}} \end{matrix} \tag{2.18}$$

This velocity can also be used to derive a function for the coagulation time of two particles depending on the initial distance. The disadvantage of this equation is that the two particles need to be aligned in the same direction as the acoustic wave is.

2.5. Other acoustic coagulation drivers and its relevance

Besides the mentioned orthokinetic particle interaction and the acoustic wake effect, other physical phenomena are likely to influence coagulation of aerosols under the influence of ultrasound. Their physics are not modeled in this work, but it is assumed that they are causing a refill mechanism, which is assumed to exist in the model discussed at paragraph 2.8. Other potential particle drift and coagulation mechanisms are inhomogeneity of the sound field, increased sound absorption by the medium, acoustic circulation and acoustic turbulence [21, 22].

2.5.1. Acoustic radiation

An object which is subjected to a sound wave will scatter the sound wave, in which it appears that the object itself is radiating the resulting wave. Since the resulting wave is a reflection of the incoming wave it cannot exceed the energy of the incoming wave, the returning wave in the direction of the incoming wave therefore has to be of a smaller magnitude and thus transferring a net momentum to the object which results in particle drift and local particle concentration increase[22].

2.5.2. Brownian motion

Brownian motion is an important coagulation mechanism for very fine particles [47] and is independent of the fact if an acoustic wave is applied[48]. Therefore it is not further investigated in this research.

2.5.3. Asymmetric vibration in a standing wave

In a standing wave, the nodes and antinodes of a wave are fixed in a position in space, but since acoustic waves are longitudinal, the medium itself oscillates along the direction of the wave. A particle at the exact antinode of the wave will therefor move towards one of the nodes during one of the half acoustic cycle. The second half cycle will force the particle to reverse its velocity. Since the particle is not exactly on the antinode anymore it will move with a lower velocity as in the first half cycle, causing a net displacement after one acoustic cycle. This effect of asymmetric vibration will cause an increase in particle concentration at the nodes of the standing wave.[22]

2.6. Modeling acoustic coagulation of aerosols

A statistical model for the acoustic coagulation of aerosols is made by dividing an input particle size distribution into fixed bins in which it is assumed that all the particles in one bin have the same size. A kernel is defined as the probability that two particles will collide depending on the particle size of both particles. This method was first developed by Smoluchowski for the modeling of Brownian coagulation[49]. For each particle bin a differential equation can be set up:

$$\frac{dn_i}{dt} = creation - destruction \tag{2.19}$$

The creation of a particle is always linked to the destruction of two particles in smaller bins, which have the same combined volume as the created particle. The probability of particle collision is defined in the kernel matrix K. The Smoluchowski equation (For which a complete derivation can be found in Appendix C results to:

$$\frac{\partial n_i}{\partial t} = \underbrace{\frac{1}{2}\sum_{j=1}^{i-1} K_{i-j,j} n_j n_{i-j}}_{creation} - \underbrace{n_i \sum_{j=1}^{I} K_{i,j} n_j}_{destruction} \tag{2.20}$$

For this type of modeling to work, the particle volume of arbitrary bin i, has to have i times the volume of a first particle in the first bin. Assuming spherical particles it means that the particle diameter of bin i has $\sqrt[3]{i}$ times the diameter of the first particle. Thus doubling the calculation range in the diameter range increases the amount of required modeling bins with 8 and the amount of Kernel entries with 16. Another drawback of this method of modeling is that it is assumed that the agglomerates have the same shape as the two particles would have before the coagulation, which is not the case for solid agglomerates.

2.7. Assumptions

- The most doubtful assumption for this model is the fact that the particles are spherical and will continue to do so after the coagulation, a method to mitigate this will be presented at the recommendations section of the conclusion.
- Assumed is that agglomerates do not break up, Fuchs[21] argues that agglomerates created due to acoustic coagulation do not have very strong bonds and can easily break. Tiwary[29] blames this effect for the fact that in his practical experiment the concentration decreases below 7µm, increases in the range of 7-30µm, but decreases again after 30µm.
- The particles are, according to the model, always evenly distributed over the coagulation chamber, however in a standing wave, particles tend to 'drift' to the nodes[22] (also see: paragraph 2.5.3)
- The model discussed is of a batch process, assumed will be that the continuous process with residence time τ will have the same coagulation as the batch process with residence time t.

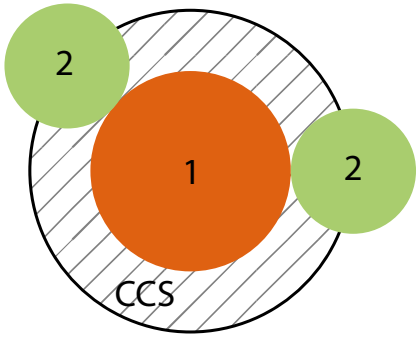

Figure 2-5: Collisional cross-section

2.8. Orthokinetic kernel

The orthokinetic kernel is based on the BFH entrainment ratio from paragraph 2.3.1, in which particles with a different size have different entrainment ratios and thus experience a relative movement. A collision volume is defined as a

cylindrical shaped coagulation volume/time which consists of a time-averaged relative particle velocity and a collisional cross-section. The collisional cross-section is defined as the area in which two particles can collide[17, 43]. In some literature, a critical offset is defined in which the smaller particles just flow around the bigger particles if they are not lined up well enough in the direction of the vibration[22, 45, 48].

$$CCS = \frac{\pi}{4}\left(d_1 + d_2\right)^2 \tag{2.21}$$

The height of the cylinder is defined by the time averaged relative velocity. From the entrainment ratio and phase difference defined in equation (2.15) and (2.16), the relative velocity can be calculated[38]:

$$u_{rel} = \left|u_i - u_j\right| = V\frac{\left|\omega\left(\tau_i - \tau_j\right)\right|}{\sqrt{1+\omega^2\tau_i^2}\sqrt{1+\omega^2\tau_j^2}}\sin\left(\omega t - \phi_i - \phi_j\right) \tag{2.22}$$

This equation still is time depended, which is inconvenient for the proposed kernel modeling. Temkin solves this by taking the time average of an acoustic period by replacing $\sin\left(\omega t - \phi_i - \phi_j\right)$ with $\left\langle 2/\pi \right\rangle$ [38, 43], which can be done because the time scale on which the coagulation takes place is much larger than that of the acoustic wave.

The coagulation volume for 2 particles of an arbitrary size is thus determined by multiplying the collisional cross section with the time averaged relative velocity. Some authors also add hemispherical end caps to this volume[43, 50].

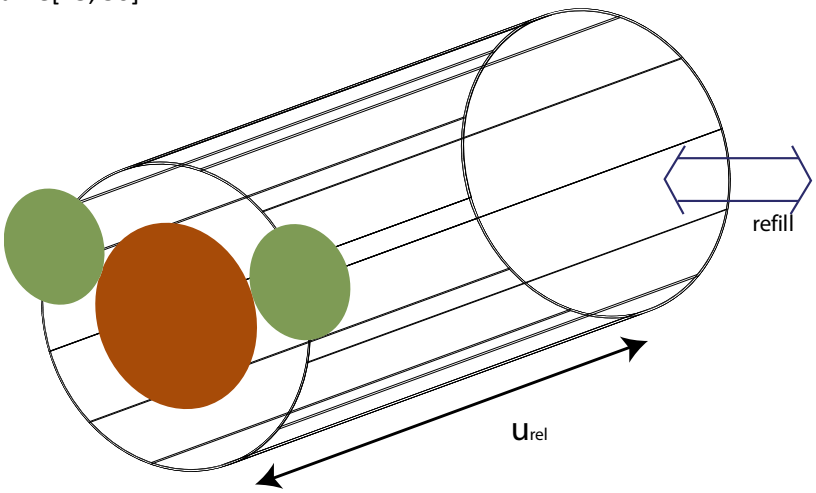

Figure 2-6: The coagulation volume with the collisional cross section as a base, and the relative velocity as length.

The coagulation volume is 'swept clean' by the bigger particles which collide with all the small particles inside the volume. This would mean that after one acoustic cycle all the bigger particles would be in solitude, however this model assumes that after agglomeration the coagulation volume is 'refilled' with particles, for which turbulence, wave scattering, Brownian motion, gravity and asymmetric vibration could be the mechanisms[17, 22].

The equation for a single kernel entry is thus:

$$\left\langle K_{i,j} \right\rangle = CCS\left\langle u_{rel,i,j} \right\rangle E_{i,j} S_{i,j} \tag{2.23}$$

In which CCS is the collisional cross section, u_{rel} is the relative velocity, E is the collision efficiency and S the fraction of the collision which will produce coalescence. In this work E and is both S set to unity

and its effect are thus ignored, which means that every collision suggested by (2.23) will take place and will lead to coagulation. The orthokinetic kernel has zeros on its main diagonal, because 2 particles with the same size have no relative velocity and thus no coagulation volume, meaning that in a monodisperse particle distribution no coagulation will take place.

2.9. Acoustic wake kernel

Hoffmann et al. proposes the use of an 'external refill factor' based on the acoustic wake effect for the orthokinetic kernel. He defines the coagulation time due to the acoustic wake effect and uses this to locally increase the particle concentration[43].

In this work, the acoustic wake effect is modeled by using Dianov's simple solution (see paragraph: 2.4) which gives a relative velocity based on the separation and sizes of two particles. The computational disadvantage of this method is that due to the coagulation of the aerosols, the particle distance increases and thus should the kernel be recalculated on every time step. The Kernel calculation scheme is therefore expanded a little. The kernel is multiplied by the particle distance to make this drop out and at every time step the average particle distance needs to be calculated so it can be used for the kernel calculation:

$$K_{aw}D = CCS\frac{3V}{4\pi\cancel{D}}\left(d_i l_i + d_j l_j\right) \tag{2.24}$$

For the particle distance needed for the acoustic wake kernel, an estimation is made by assuming that all the particles are aligned in a cubical grid and that the distance between the particle is bigger than the particle diameter:

$$D = N^{-1/3} \qquad \left(d/D << 1\right) \tag{2.25}$$

2.10. Input particle size distribution

The initial size distribution for the model is the measured distribution from the practical experiment. The used measurement device (see: paragraph 4.1.1) is not able to measure particles with a size smaller than 0.3µm, however from the cut-off in the measurement it can be assumed that that there is a relevant amount of smaller particles which are not measured. For most occurring aerosols sources, the particle size distribution can be fitted with the Log-Normal distribution[16], but the normal distribution is also considered[1]:

$$pdf_{normal}\left(d\right) = \frac{1}{\sigma\sqrt{2\pi}}e^{-\frac{\left(d-\mu\right)^2}{2\sigma^2}} \qquad pdf_{\log-normal}\left(d\right) = \frac{1}{d\sqrt{2\pi\sigma^2}}e^{-\frac{\left(\ln d-\mu\right)^2}{2\sigma^2}} \tag{2.26}$$

[1] The Weibull/Rosin Rammler distribution was also considered but is not documented in this report.

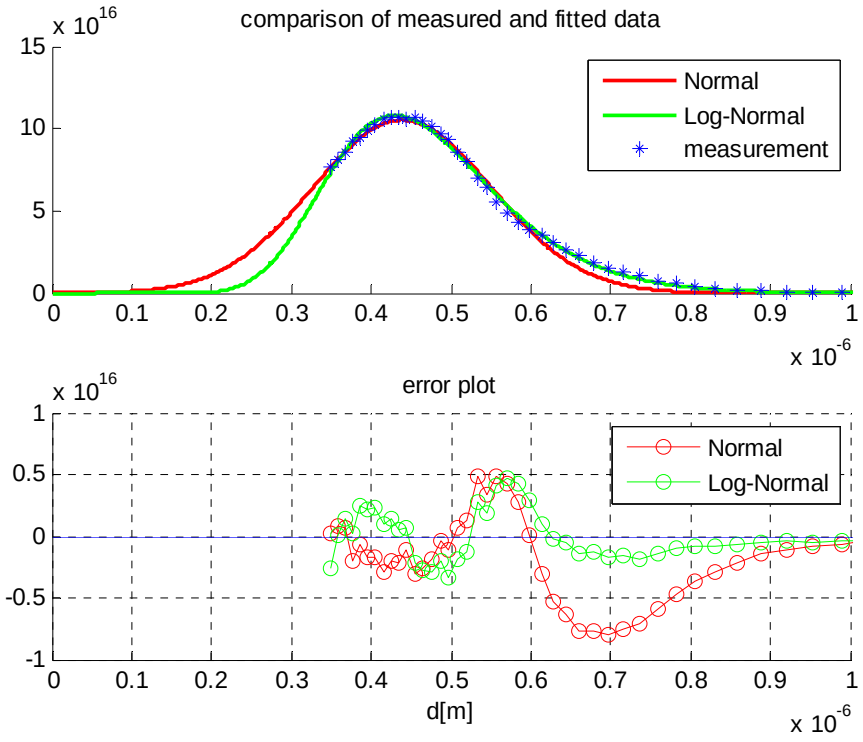

Figure 2-7: Input particle size distribution, which is from a measured aerosol source and extrapolated with the help of a statistical distribution.

A fit for both the distributions was made and fitted for the total number density, mean value and standard deviation to get a lowest possible total deviation over the entire particle size range. It can be seen that the log-normal distribution has a closer match to the measured values. This is an important conclusion if looked at the difference between the two distributions outside the measurement range, which is where the extrapolation is applied.

2.11. Modeling routine

The modeling equations are implemented in MATLAB, for which the code can be found at appendix E. The MATLAB solver ode45.m was used to compute the solution of the system of differential equations. The model routine is shown in Figure 2-8.

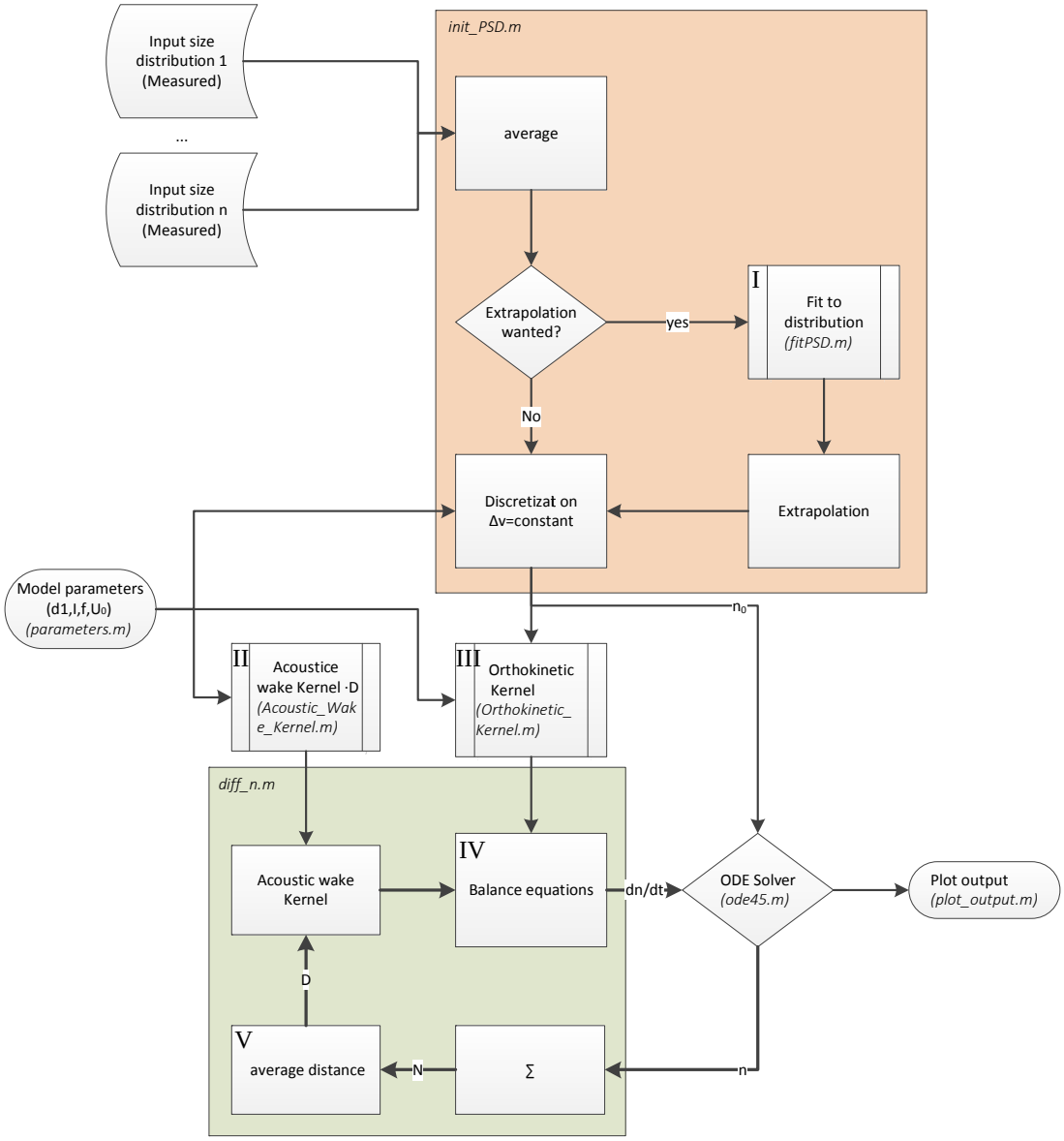

Figure 2-8: Kernel modeling scheme to model the whole acoustic coagulation process, the file names of the MATLAB are indicated in italic and parenthesis. The roman numbers indicate equation references:
I: Statistical distributions (2.26)
II: Acoustic wake effect kernel (2.24)
III: Orthokinetic kernel (2.23)
IV: Smoluchowski model equation (2.20)
V: Relation between particle concentration and particle distance(2.25)

3. Practical approach: ultrasonic radiation source

3.1. General description

Nowadays and in this practical research, the macrosonic transducers are of the Bolt-clamped Langevin-type transducer (BLT)[7] which operates in resonance and are thus designed for one or a limited amount of frequencies. In the 1950s and 1960s the experiments were performed mostly with whistles and sirens offering a high power output, but with a low efficiency[22]. Modern BLT transducers use the piezo-electric effect of a lead-zirconate-titanate (PZT) ceramic material. Piezo-electric materials deform under the influence of an electric field [51].

Figure 3-2-1: Disassembled transducer

The transducer used in this setup is from a company called Clangsonic which sells it for the use of ultrasonic cleaning. The induced pressure fluctuations in the liquid results in cavitation which can remove dirt from small crevices and is used for example jewelry. The device was taken apart and its geometry measured and modeled. One modeling option considered is to derive an equivalent electronic circuit and model that using appropriate software[52]. Earlier works show that working with finite element modeling (FEM) is rewarding [53-56]. The model was validated with the use of laser Doppler velocimetry, impedance and sound pressure level measurements.

The ultrasonic transducer in this research is designed to be used in a cleaning tank filled with water. Since water has an acoustic impedance which is much higher than air, the velocity amplitude of the transducer is not sufficient to transfer enough power to an air column.

A solution for this was pioneered in the 1970s by prof. J.A. Gallego-Juarez et al.[25]. The vibration amplitude can be increased by using a stepped horn and the power is transferred to air by a radiation plate in flexural mode.

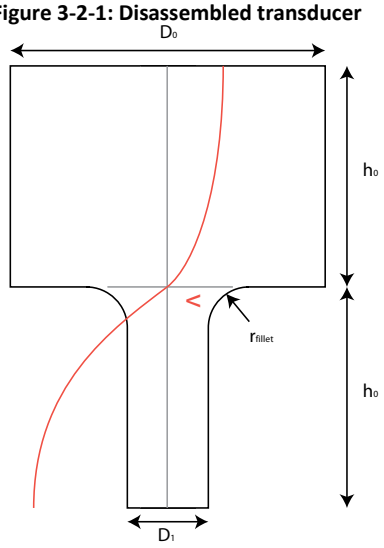

Figure 3-2: Schematic view of the ultrasonic horn, the red line is the velocity amplitude.

The horn consists of two adjacent cylinders with dimensions as shown in Figure 3-2. At the top, the horn is connected to the transducer and at the bottom the horn is connected to the radiation plate so both ends are anti-nodes. The middle of the transducer is a node which means that the total length of the horn should be half a wavelength.

The node in the middle is at rest, so there is an equal amount of momentum at the large cylinder and at the small cylinder. This means that the displacement at the small cylinder is multiplied by the ratio of its areas:

$$x = \frac{A_0}{A_1} = \left(\frac{D_0}{D_1}\right)^2 \tag{2.27}$$

The amplifier was designed using this equation which is a 2D-simplification. To make up for the difference, the resonance frequency was matched again by adjusting the fillet radius in the FEM model. Three concept designs were fabricated and tested.

Table 3-3-1: Comparison between the mechanical amplifiers, h_0 should have an equal length as h_1, however the bolt used to assemble the radiation plate to the horn is also part of the tuned length

	horn 1	horn 2	horn 3
material	Steel 9SMn28	stainless steel 316	stainless steel 316
production process	hand-turned	CNC-turned	CNC-turned
$\left(D_0/D_1\right)^2$	20.25	20.25	20.25
h_0	31.5mm	30.6mm	30.6mm
h_1		23.8mm	23.1mm
r_{fillet}	9mm	8mm	8mm

Also two radiation plates were designed, one of 0.8mm thick and having an outer diameter of 65.1mm and one of 1.5mm thick and having an outer diameter of 64.8mm, so in total six combinations will be evaluated on resonance frequency and intensity.

Figure 3-3: Two ultrasonic horns, one with a flexure mode radiation plate.

Beside the horn, plate and transducer, an Allen bolt is used to attach the radiation plate to the horn, this is far from ideal for the geometry because of the hole it leaves in the assembly and because, but is necessary to fix the radiation plate.

3.2. FEM model

For the FEM model COMSOL multiphysics 4.3 was used because of its ability to combine several types of phenomena in one user interface and calculation domain. The physic “acoustic-piezoelectric interaction, Frequency domain” was chosen because this contains the modeling of the piezoelectric effect, mechanical vibrations and is fully coupled with acoustics[57]. To save computational time, the model is chosen to be 2D axisymmetric.

The model is run with a frequency between 10 and 100kHz, with the speed of sound being approx. 340m/s, the wavelength in air has a minimum of 3.4mm, so the mesh grid is chosen to have a size of around 1mm. The wavelength in the transducer material is an order of magnitude higher than the wavelength in the surrounding air. Both ceramic rings have to be in the right coordinate system, because of the anisotropy of the piezo-electric effect.

One of the problems with the modeling is the material damping of the transducer. COMSOL offers Rayleigh damping or a one parameter isotropic loss-factor which is defined as the energy lost per vibration cycle[58]:

$$\eta_s = \frac{E_{lost}}{E_{total}} \tag{3.1}$$

For reasons of modeling simplicity, the one parameter option was chosen. Increasing the damping results in a decrease of the amplitude in the resonance peaks, but not in a change of the resonance frequency.

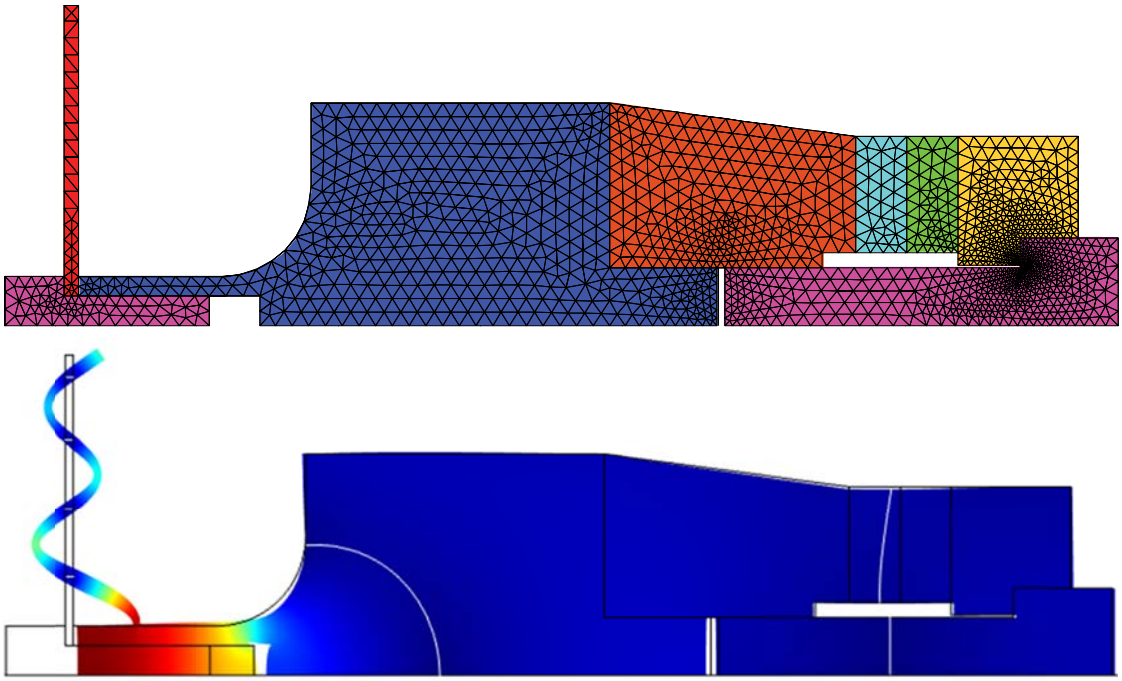

Figure 3-4: Transducer assembly as modeled in COMSOL. Above: Mesh of transducer, the individual parts are a bolt (2x magenta), top weight (yellow), piezo-ceramics (green and blue) transducer bottom (orange), horn (dark blue) and the radiation plate (red). Below:

3.3. Measurement methods

To validate the COMSOL model a few measurement methods were used. Together with the manufacturer specifications of the transducer a validation of the transducer could be acquired.

3.3.1. LDV measurements

A measurement was performed with the laser Doppler vibrometer (LDV) to validate the resonance frequencies. The transducer was connected to a RF A-class amplifier (ENI2100L) which in turn was driven by a laboratory signal generator. Because of the high frequency of the signal and the sudden availability

of the other equipment, the data acquisition was done by an oscilloscope and put into the computer by hand.

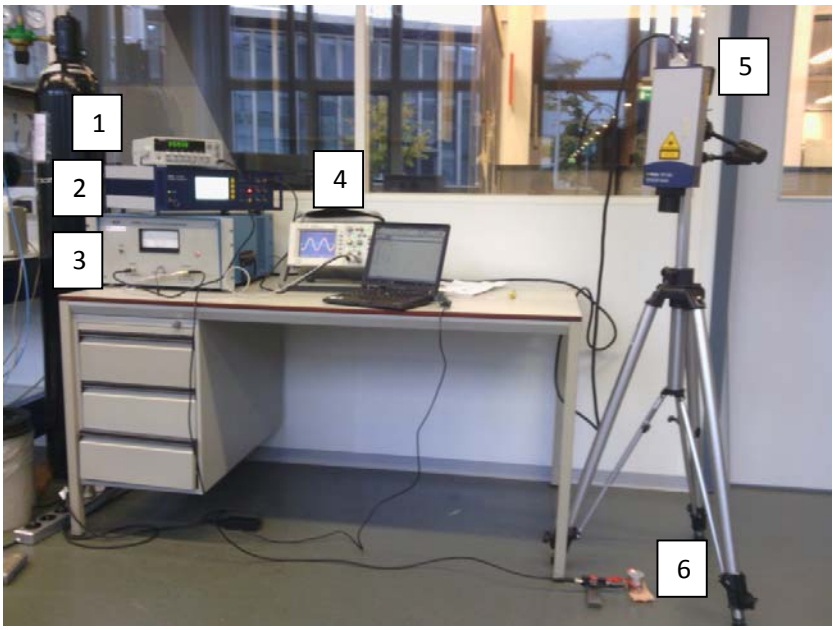

Figure 3-5: Transducer measurement setup with: 1)Signal generator 2)Polytec OFV-5000 LDV controller 3)ENI 2100L RF power amplifier 4)Oscilloscope for data acquisition 5)Polytec OFV-505 LDV measurement head 6)Ultrasonic transducer.

3.3.2. Impedance measurements

The resonance mode of the transducer also results in a decrease in electrical impedance. Therefor a Wayne Kerr 6400B Component analyzer was used, which can measure the impedance and the phase difference of the transducer for predefined frequencies. With this information the net electrical power uptake by the transducer can also be estimated for a given voltage. The equivalent capacitor value can be found by measuring the impedance outside the resonance frequencies in which the phase is -90°.

3.3.3. Sound pressure level measurements

Also the sound pressure level was measured using a calibrated test microphone. The resonance can be found by sweeping the frequency and measure the resulting sound pressure level. A translation between the sound pressure and the velocity field is described by the acoustic impedance which is further elaborated in Appendix B.

3.4. General practical considerations

Also first practical experience from these test setups were of importance for further experiments done.

- Improper shielding of the cable between the amplifier and the transducer can lead to unexpected behavior of the measured voltage and the use of coaxial cable is thus desired.
- For capturing the proper resonance frequency, the use of a signal generator which can be fixed at a desired frequency is important not only for the stability of the resonance point, but also for the repeatability of the experiment.
- The output voltage of the amplifier decreases significantly if the transducer is in one of its resonance modes, because of the amplifiers output impedance of 50Ω. Knowing this, the

resonance point can be found without using external instruments, but by sweeping the frequency to find a local minimum in the voltage.

3.5. Transducer model validation

For a first model comparison, the velocity amplitude was measured with the LDV in frequencies ranging from 10 to 100kHz. The measured frequency was swept to ensure that the resonance peaks are grasped in the graph. In the COMSOL model the damping was varied to match the measured displacement velocity:

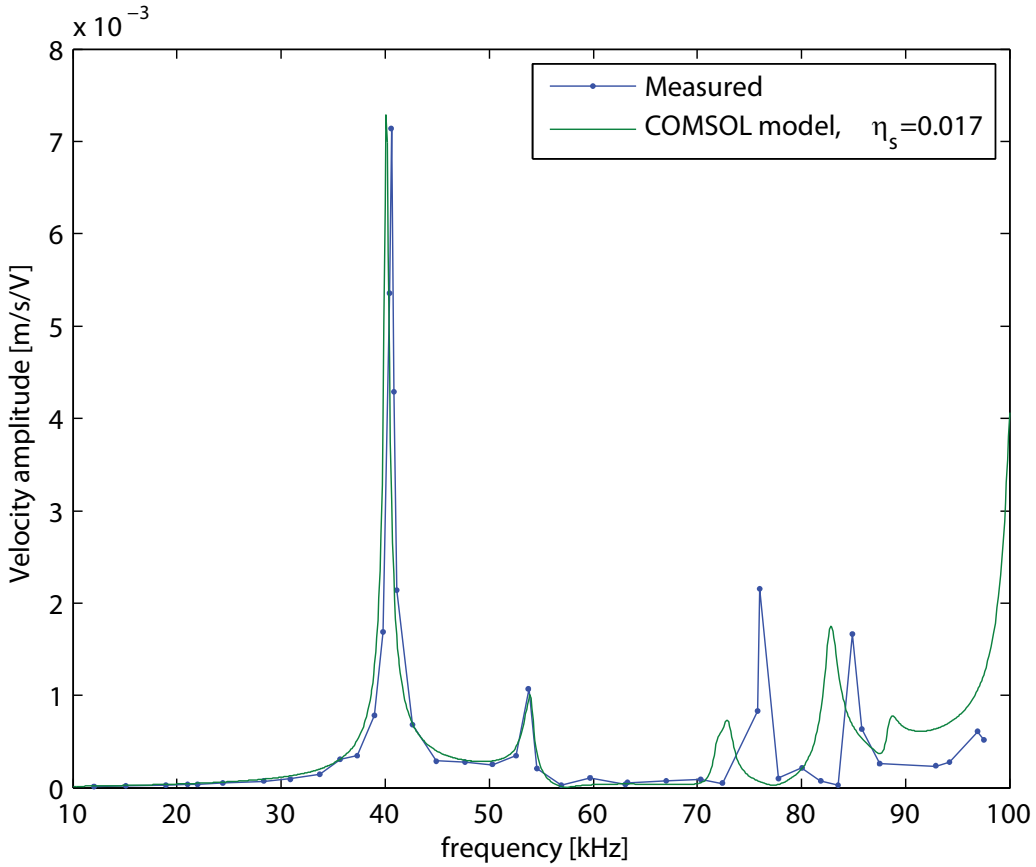

Figure 3-6: The frequency response measured at the bottom of the transducer compared to the output of the COMSOL model. The damping determined by the isotropic loss factor is determined by varying it by trial and error.

In the graph the y-axis shows the velocity amplitude in m/s/V, which implies the relation between input voltage and displacement to be linear, which is exactly the case for the COMSOL model. The consequence of this is that measurements done with different input voltages can be compared. The relation was verified in practice at a frequency at which the transducer is not a resonance and shown in Figure 3-7.

The model is a good representation in the region of the first two resonance peaks. However it fails to match up with the behavior of resonance modes above 70kHz. Possible reasons for this can be that the vibration is not axisymmetric anymore or that the shape of the model should be further refined in the FEM model.

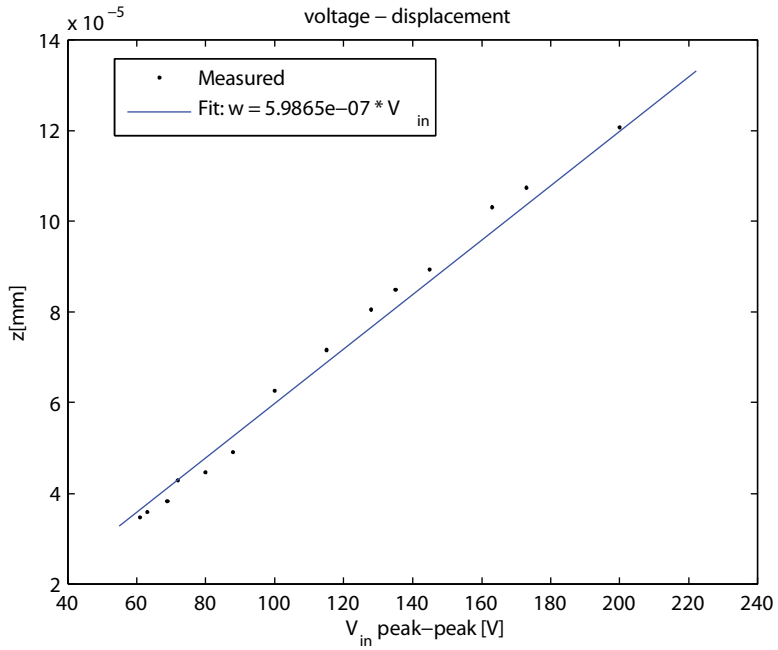

Figure 3-7: Measurement of the relation between the input voltage and the displacement at the bottom of the transducer. Due to the instability of the oscillator the frequency is within a range of 44.4 and 44.7 kHz.

By combining all the measurement data, a comparison can be made between properties specified by the manufacturer, the COMSOL model and the various measurements, it can be seen that the model is an accurate description for both the specifications and the various measurements.

Table 3-2: A comparison of transducer manufacturer specifications, FEM modeling results and measurements. The voltage in the table for the velocity amplitude is based on the manufacturer's data stating that the transducer is rated at 60W while having 20Ω impedance.

	Specified by Clangsonic	COMSOL model	LDV measurements	Impedance measurements	SPL measurements
1st resonance frequency	40+/-0.5kHz	40.1kHz	40.6khz	40.6+/-0.2kHz	40.5kHz
Impedance	20Ω @resonance	-	-	20.9 -10/+20Ω	-
Capicitance	4200pF +/-15%	-	-	3800+/-100 pF	-
Velocity amplitude	0.5m/s	0.35m/s (@34.6Vrms)	0.35m/s (@34.6Vrms)	-	0.75-1m/s @max voltage

3.6. Selection of horn and radiation plate for air coupling

From the six different combinations of three horns and two radiation plates, the two combinations which use the steel horn the best performing in terms of measured displacement amplitude. With the steel horn and the 0.8mm radiation plate the sound pressure level increased from 146dB to 153dB which is a 7dB gain and thus a more than doubling of the velocity amplitude. However the resonance frequency also increased from 40.6kHz to 41.0kHz, in the later state of the practicum this frequency even increased up to 41.8KHz.

If looked at the bode plots obtained from the impedance measurements another indication of not entirely match frequencies can be found.

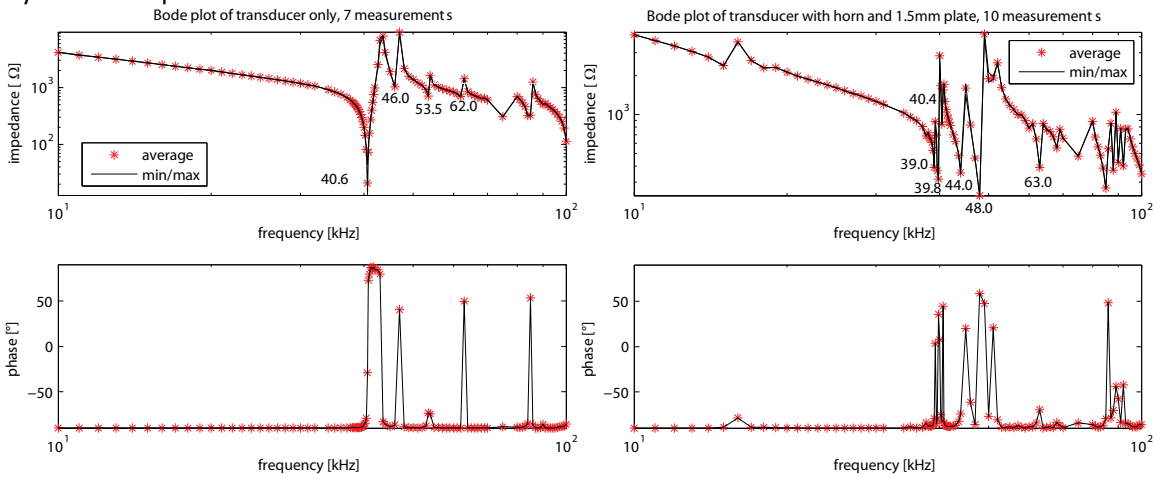

Figure 3-8: Left: Impedance measurement of the transducer shows that the impedance is 10-45Ω at 40.6kHz and the phase difference is ranging from -30 to 30, the measurements outside the resonance do not show this high uncertainty. From the impedance outside the resonance points the capacitance can be calculated.
Right: Bode plot of the transducer with steel horn and 1.5mm radiation plate. Comparing this plot with impedance measurement of the transducer it can be concluded that there is an increase in the amount of resonance modes which have higher impedance, this could be because of slight differences in the resonance frequencies of the transducer, horn and radiation plate. This suggests that there is room for improvement in the resonance tuning of the horn and radiation plate.

4. Practical approach: Small scale acoustic coagulation of aerosols

With the designed and optimized ultrasonic transducer for gas media, a test setup was designed to evaluate the potential of the coagulation process. The test setup roughly consists of an aerosol source, the coagulation chamber and a particle size measurement device.

4.1. Measuring particle size distributions

There are a few methods for measuring particle size distributions relying on different physical phenomena regarding aerosols.

Cascade impactor[59, 60]:

Particles will flow through a chamber with is obstructed by an impact plate. Small particles will follow the streamline of the flow around the plate, while big particles will collide with the impact plate. Counting the amount of impacts on a plate and measuring the flow tells something about the concentration of particles with a high enough aerodynamic diameter. A cascade of impactors can give a particle size distribution. A detection system on the impact plate is also required.

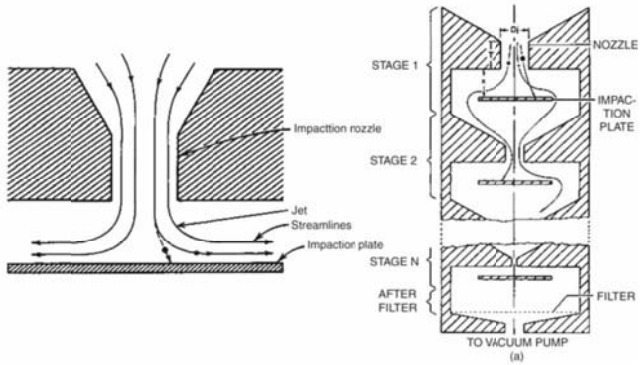

Figure 4-1: Overview of the cascade impactor, on the left a single stage is shown. Particles collide with the impaction plate depending on their aerodynamic equivalent diameter, density, nozzle size and distance between the nozzle and the impaction plate[59].

Optical particle counter (OPC)[59]:

Aerosols flow through a laser beam in which the particles cause the light to scatter. The scattered light is received by a photodiode and the scattering angle and intensity depends on the size, shape and refraction index of the particle[61]. The OPC collects the scattered light over an angle which is defined by its optical design. The intensity of the scattering is translated to the size of the measured particle.

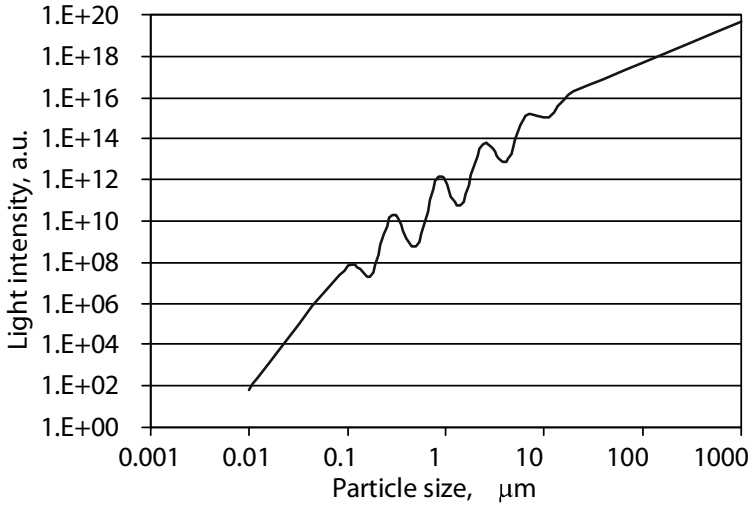

Figure 4-2: light scattering of aerosols, the region below 0.1μm is the Rayleigh region in which is the intensity is to the 6th power (volume squared) of the particle size. The fluctuations between 0.1 and 30 μm is called the Mie region, which unfortunately the region of interest, and above 30μm the intensity is related to the cross-section of the particle [62](Rayleigh scattering)[59].

Differential mobility analyzer (DMA)[59]

The aerosol is led through a radioactive source to make sure the particle charge is known and is then fed into to a chamber with a controlled electric field. The particles with the same electrical mobility (mono-disperse) exit the chamber and need to be counted by an external instrument. A particle size distribution can be obtained by scanning the intensity of the electric field and counting the mono-disperse particles.

4.1.1. TOPAS LAP320[63]

The particle size classifier used in this research is an OPC from the German brand TOPAS, which can measure particles in a ranges from 0.3-20μm with concentrations of up to 10^{11} particles/m^3. The mean reason this device was chosen is that it can handle high aerosol concentrations, has a measurement range useful for this research and is very user friendly. The device takes in 3L/min from which only a small part is led through the part of the apparatus which does the actual particle size measuring. This part is described in Figure 4-3.

The signal from the photo sensor is divided into logarithmic classes and the count per class is transferred to the computer which is connected to the OPC. The calibration is loaded into the computer and assigns a particle size range to a class from the OPC. Calibration is done regularly by running the device with several monodisperse aerosols with known size and is needed to mitigate the fouling of the optical system and the deterioration of the laser.

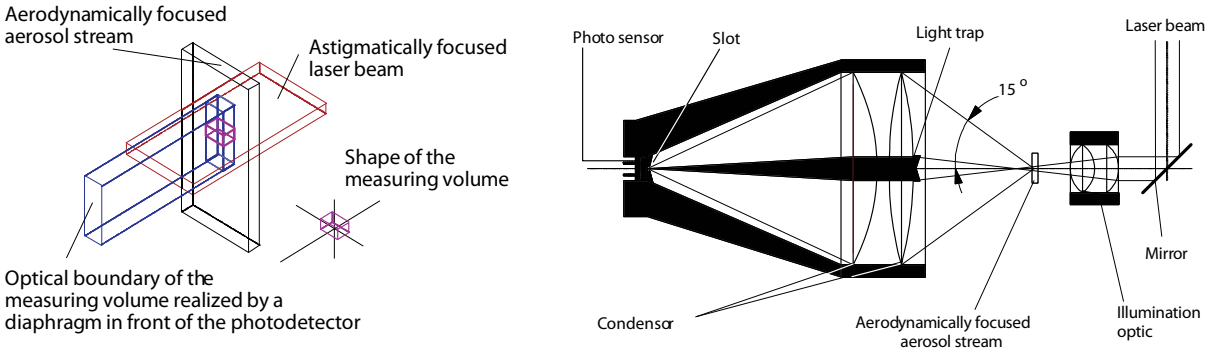

Figure 4-3: Principal working of the optical particle counter used in this research. Left: Sheath air is used to aerodynamically focus the aerosol stream, this and the optical boundaries form the measurement volume. Right: The scattered laser light is collected by a lens to be focused on a single photo detector[63].

The uncertainty from measuring the scattering intensity of particles near the wavelength (See: Figure 4-2) of the light used can be mitigated by using different scattering angles. Even backward scattering can be used. However the effect of having irregular shapes remains uncertain. The forward scattering at different angles for spherical and non-spherical are shown in Figure 4-4. An elaboration on different equivalent diameters can be found at Appendix D.

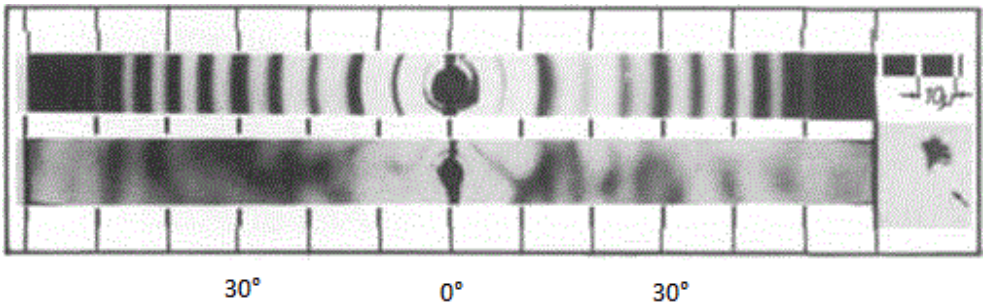

Figure 4-4: Scattering intensities of 2 particles with roughly equal dimensions, but different shape. The top particle is glass sphere and the bottom is an irregular shaped quartz crystal.[64] The OPC used in this work has a scattering angle of +/-15°.

4.2. Artificial aerosol source

For the experimental setup an artificial particle source should meet a few requirements to get satisfactory results, the following were used for this research in this order of importance:

1. Repeatability. Besides the fact that a repeatable experiment is of a higher scientific credibility, the experiments have to be repeated for the case with and without ultrasonic treatment.
2. Continuous operation. This is one of the requirements of the setup, because this eliminates the fact that untreated aerosols are inside the tubes from the beginning of the experiment.
3. Size distribution ranging from 0.3-2.0µm. The minimum is set by the measurement capability of the OPC and the maximum is set by the fact that the research focusses on sub-micron particles (see: chapter 1), so the preference is in the lower region of this distribution. Narrow size distributions are favorable due to modeling implications (See: paragraph 2.10).
4. Availability. The first three options are important, but if the suggested approach is not available and too expensive to acquire it is still no viable option.

5. Resemblance of flue gas. Looking ahead to the applications of the suggested technology the feasibility can be better evaluated if the used artificial aerosol has more common properties with 'real' flue gasses or gasification syngas.

A few options were considered:

Cigarette smoke mostly consist of tar droplets with a particle size of around 0.15-0.5µm [65, 66] and since it is a plant based combustion sourced particle it bears resemblance with common flue gasses. The problem is however that burning a cigarette is a batch process by design and it is unsure that the process of lighting a cigarette can be done in a way which makes the aerosol concentration repeatable, also a continues mode is not possible for obvious reasons.

Fog machines are artificial aerosol sources used for entertainment purposes such as theaters and rock concerts. The machines interesting for this research are classified as haze machines which produce a fog with a smaller particle size (between 0.1 and 1.0µm[67]) and is less dense and fades slower. The haze is made by dispersing mineral oil under high pressure. The disadvantages are high costs (although there is a possibility to rent one, which also requires extra planning) and high flow rate of aerosols which could be easily mitigated by diluting.

Electrospray crystallization is a method for creating submicron crystal particles by spraying a liquid solution from a charged nozzle towards a grounded plate[68]. The particles have a unipolar charge so will not agglomerate at the production. To make the particles agglomerate in the chamber, the charge of the particles should be neutralized with a bipolar charge neutralizer such as used in the electrical mobility analyzer discussed at paragraph 4.1.

Conductive or semi-conductive materials can be created used to create an aerosol using high voltage spark discharge in a gas stream. Because of the high temperature spark, the material of the electrodes evaporates from the electrodes and condenses back into the gas stream. The particle size which can be obtained is in the size order of 1-10nm. For instance the primary particle size of gold particle is 1.3nm[69] and depending on the gas flow and spark characteristics, coagulation takes place before condensation of the particles.

Incense consists of wide variety of resins, woods, bark, seeds, essential oils and synthetic chemicals design to produce a fragrant smoke. The smoke consist mostly of (4-ring) PAH's[70]. The particle size peak is in the 0.26-0.65µm[71] range, depending on the type and composition of the incense.

Atomization is a process in which a fluid is forced through a nozzle by a pressure difference. The droplet size distribution can depend on the pressure difference, fluid properties and nozzle design, but if oil is used the size range is in the order 0.5-5.0µm[22]. A few tests were done with an atomizer which was built at the faculty of chemical engineering at the TU Delft using three different oils and a brine solution. Instrument air was used to drive the atomizer and the aerosol flow rate can be adjusted by regulating the pressure. The OPC is taking up no air when it is not running and 3L/min if it is running so a filtered ventilation connection was placed in line with the atomizer and the OPC.

The following oils were used in the atomizer in order of increasing viscosity:

1. Paraffin oil intended for lamps from 'Kruidvat' brand which have a carbon chain length between 5 and 20 C atoms.
2. 'Shell' 10W40 standard motor oil.

3. ‘Hema’ 15W50 motor oil which is a bit thicker and is intended for older engines that leak oil.

The properties of the aerosols created by atomization depend on the pressure which is shown in the following table:

Table 4-1: Atomizer test run from which is concluded that the best pressure range for the atomizer is between 1.25 and 1.5 bar to maintain a steady flow and consistent particles size.

pressure	flow	concentration	mean particle size	remarks
0.75bar	1.2L/min	NA	NA	no atomization
1bar	1.45L/min	2100+/-100 particles/cm^3	0.670+/-0.005µm	irregular atomization
1.25bar	1.65l/min	4300+/-150 particles/cm^3	0.745+/-0.005µm	
1.5bar	1.83L/min	5100+/-50 particles/cm^3	0.755+/-0.005µm	max pressure for glass bottle

The atomizer can also be used to produce solid particles by spraying a salt solution, assuming that the used instrument air is dry, the brine droplets crystalize in the air forming solid crystals. The particle size depends on the size of the droplets and the salt concentration in the solution.

Table 4-2: Difference between the three different aerosols created by using liquids at 1.5bar pressure. Based on this experiment it was decided to use the Paraffin from Kruidvat to create an aerosol containing droplets, because of high particle concentration which creates a visible fog, and the brine solution for solid particles.

liquid	concentration	mean particle size	remarks
Kruidvat	70500+/-500 p/cm^3	1.235+/-0.005µm	Mono-disperse with a peak at 1.67µm
Shell	5100+/50 p/cm^3	0.755+/-0.005µm	Wide dispersity with a high amount of particles in the region 0.3-1µm and a lower amount in the 1-3µm region.
Hema	2800+/-50 p/cm^3	0.580 +/-0.01µm	Wide dispersity with a high amount of particles in the region 0.3-1µm and a lower amount in the 1-3µm region.
Brine	61500+/-500 p/cm^3	0.540+/-0.01µm	PSD used in paragraph 2.10

Table 4-1 and Table 4-2 show satisfactory results regarding the requirements set at the beginning of this paragraph and are thus used throughout the experiments.

4.3. Coagulation chamber

For visibility the chamber was made from a PMMA tube with an aluminum bottom and top. The transducer assembly was mounted with a rubber gasket at the velocity node of the horn to ensure that a minimum amount of energy is lost at this attachment and the radiation plate is securely fixed in the center of the tube without hitting the wall. Another advantage of this fixation is that the wire leads of the transducer are on the outside of the setup.

The whole chamber is working at near atmospheric pressure, mainly because the OPC should have no flow induced at its entrance. Yet still the chamber was tested for leaks at up to 2 bar to make sure the operation is safe outside a fume hood which eases the operation of the experiment.

The piston inside the chamber acts as a reflector. By reflecting the incoming wave a standing wave is created by adding the incoming and reflected waves.

For this to happen, the length of the chamber needs to be tuned which is why the reflector is movable like a piston. The top of the chamber is a velocity node and a pressure antinode. A small piezoelectric transducer similar to one used in a greeting cards with music is used to measure the pressure waves at the reflector. The piston height is controlled to find a local maximum for this pressure amplitude to make sure a standing wave is achieved.

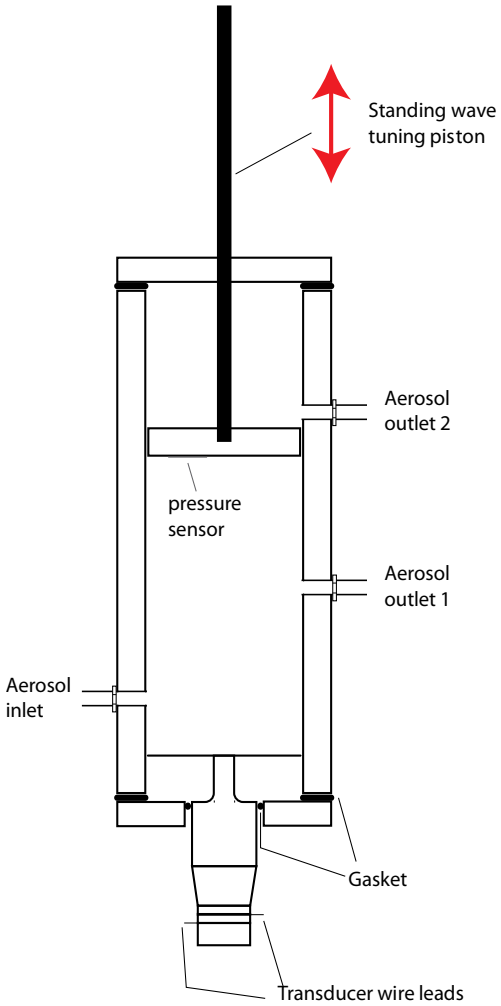

Figure 4-5: Coagulation chamber with transducer.

Another function of the piston is to control the volume of the chamber and thus the residence time of the aerosol. If the piston is set to the point that the chamber is large it would mean that the outlet is relative close to the inlet, so that the residence time for some of the aerosols could be very short. One of the outlets is always blocked.

4.4. Practical setup

The practical setup is consists of the hardware discussed in the previous paragraphs and some auxiliary devices. In order not to lose aerosols due to static charge build up, all the pipes are made from stainless steel and the hoses are electric conductive. Also the layout is designed in such a way that the aerosols do not pass through valves.

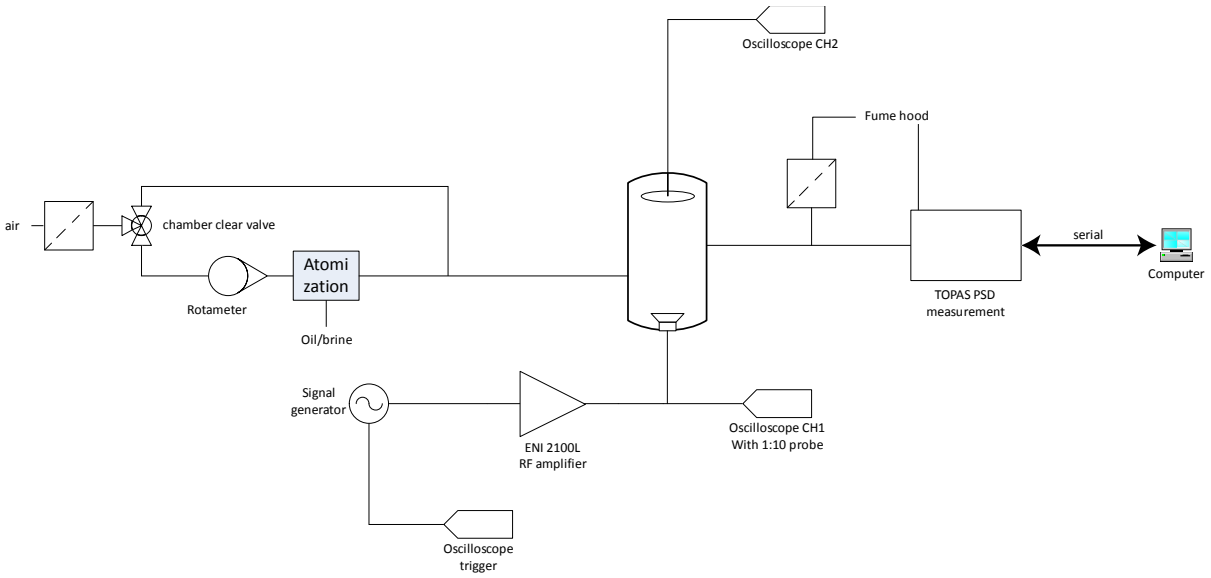

Figure 4-6: Process diagram for the small scale acoustic coagulation of aerosols.

There are two control parameters for the process which effect the gas flow, the valve which controls the air supply, the OPC and the ultrasound, the following operating modes of the setup can be distinguished:

Table 4-3: Different flow configurations of the practical setup.

chamber clear valve	OPC	operating mode
to atomizer	on	PSD measurement
to chamber	off	clearing chamber of 'old' aerosols
off	on	OPC cleaning (air is taken from the fume hood through a filter)
to atomizer	off	aerosols are being produced but are directed to the fume hood

The data acquisition was partly done by the computer via the OPC and partly by the oscilloscope. The oscilloscopes internal digital filter was used to improve the signal from the pressure sensor from which the cleanliness of the signal can be recognized on the picture of the setup (Figure 4-7). The ability to read voltage amplitudes directly from the oscilloscope also improved the ease of data acquisition.

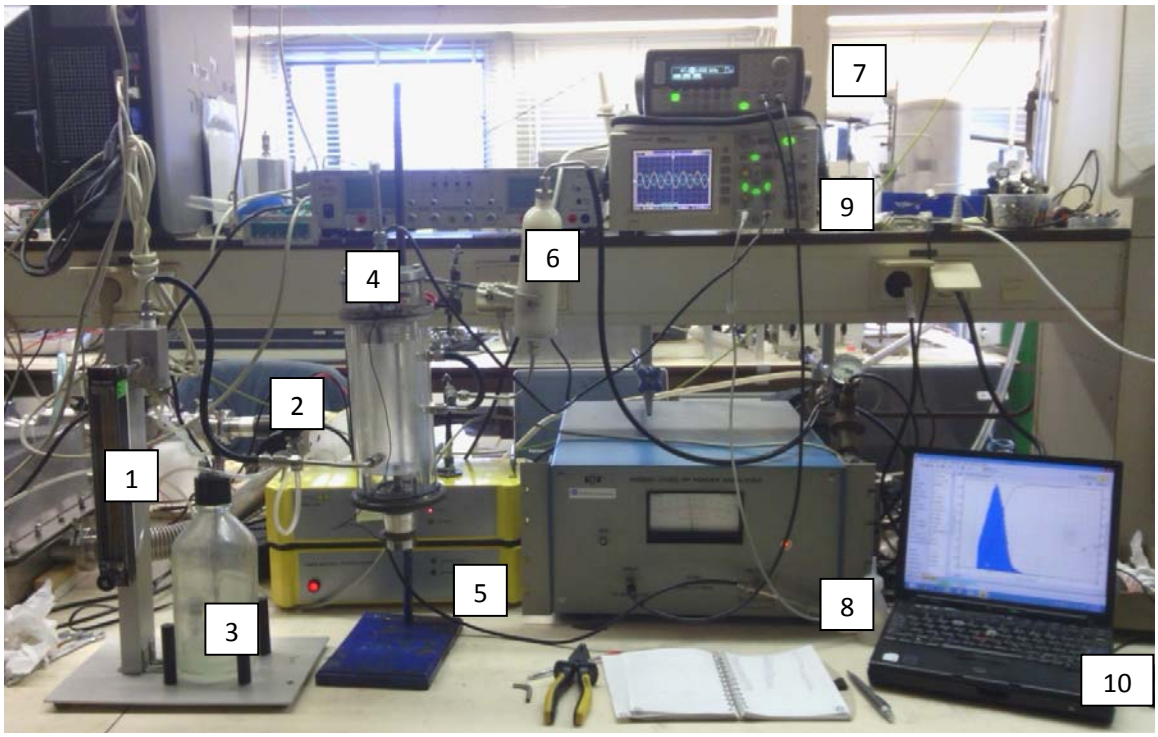

Figure 4-7: Practical acoustic coagulation setup with: 1) Rotameter 2)Chamber clear valve 3)Atomizer 4)coagulation chamber 5)OPC 6)HEPA filter 7)Signal generator 8)RF amplifier 9)Oscilloscope 10) computer for data acquisition

5. Results

5.1. Variables

Three experiment series were done with the setup described in the previous chapter. The computer model was run with the parameters which resemble the measured input parameters for the process as much as possible.

5.1.1. Sound intensity

Unfortunately, calibrated in situ SPL measurement is not available in this setup, but the small piezo transducer at the reflector gives a voltage to depending on the pressure oscillation. The value of the voltage amplitude can be used as an indication of the sound pressure level inside the chamber and is listed in Table 5-1. However at large transducer voltages (>150V_{pp}), the frequency of the signal from the pressure sensor tended to double or even triple, which could indicate harmonics caused by non-linear acoustics (see: Figure 5-1, paragraph 2.1).

After an initial tuning of the transducer's resonance and standing wave, the signal of the pressure sensor decreased after a few minutes of operation, also the voltage of the amplifier increased which indicates an increase in impedance. A probable explanation for this is the heating up of the transducer, which can be clearly felt at the horn after a few minutes of operation. The heat could change the physical properties of the material and thus alter the resonance frequency of the transducer.

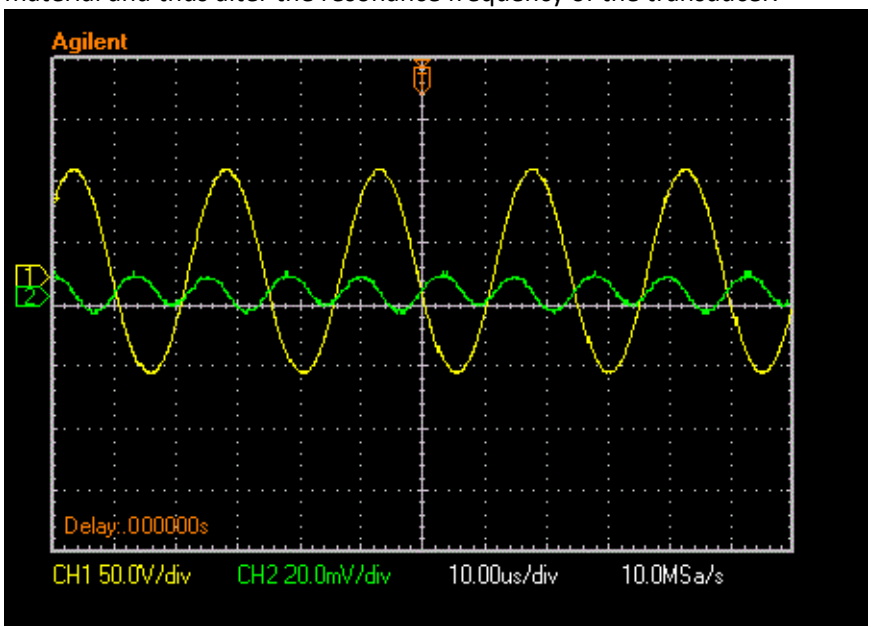

Figure 5-1: Image export from the oscilloscope during an experiment. The yellow line is the signal to the transducer showing a period of approximately 25µs (40kHz). The green line is the voltage from the pressure sensor which appears to have a frequency twice that high.

For these reasons the sound pressure level cannot be better estimated than being in the range of 150-160dB, 153.7dB was the maximum sound pressure level measured with the calibrated microphone. The voltage on the transducer was increased in the actual setup. Also the measured value was in the free field while the final setup was with a standing wave which theoretically should double the velocity

amplitude. For these reasons, the modeled acoustic field was assumed to have a velocity amplitude of 2m/s, which corresponds to roughly 149dB which is a moderate value in the field of macrosonics[72].

5.1.2. Residence time

The required treatment time of the aerosol is of great importance for the potential of the proposed technology, because it has a direct relation to the size of the coagulation chamber. The residence time in the experiments was determined by the volume flow measured by the rotameter. Assumed is that the residence time of all the particles can be calculated by dividing the volume of the coagulation chamber by the flow rate, which is one of the assumptions for the model.

5.1.3. Discretization

The division of the particle distribution in measurement bins is determined by two parameters, the particle size in the first bin and the amount of bins. The relation between these parameters and the rest of the bins is shown in chapter 3. The smallest bin is chosen to represent the smallest value of the input size distribution which has a significant particle concentration.

The amount of bins is limited by the computer running the simulation. 8000 bins require two matrices (for each kernel one) of 8000^2 values, so with MATLAB taking 64-bits per value the required internal memory scales quadratic to the amount of bins. Note that an increase in the first particle bin results also in an increase of the last particle bin, but an increase in the amount of bins only leads to cubic root increase in range, so a good trade-off should be found for the model.

5.2. Model validation

The model will be validated for three cases, one measurement series with oil droplets as an aerosol and two cases with salt particles from atomizing the brine. In one measurement series helium is used instead of air to create the salt crystal aerosol. The following physical parameters are used:

Table 5-1: Comparison of the input parameters within the bounds of which was measurable and its translation to model input parameters. The amplification is the gain in voltage over the amplifier, a decrease in amplification points to lower impedance of the transducer and thus resonance, because of the output impedance of 50Ω of the amplifier.

Aerosol properties	Series 1	Series 2	Series 3
gas	instrument air	instrument air	helium
aerosol	paraffin oil droplets	NaCl crystals	NaCl crystals
particle concentration	$11.9 \cdot 10^{10}$ p/m^3	$5.8 \cdot 10^{10}$ p/m^3	$2.57 \cdot 10^{10}$ p/m^3
mass concentration	2.94g/m^3	0.24g/m^3	0.004g/m^3
residence time	22s	18s	8s
flow rate	1.59l/min	1.96l/min	4.44l/min
mode in LN fit	1.45µm	0.51µm	0.43µm
Transducer operation			
setup	steel horn/1.5mm plate	steel horn/0.8mm plate	steel horn/0.8mm plate
frequency	41.863/41.745kHz	41.880kHz	41.821
signal generator voltage	150/250mV$_{pp}$	150/270mV$_{pp}$	150mV$_{pp}$
transducer voltage	114/-V$_{pp}$	120/225V$_{pp}$	113V$_{pp}$
amplification $\cdot 10^{-3}$	0.76/-	0.80/0.83	0.75
pressure sensor voltage	20-30m/-V$_{pp}$	30/40-60mV$_{pp}$	20mV$_{pp}$

Model input			
ρ_p / ρ_f	800/1.2 kgm^{-3}	2160/1.2kgm^{-3}	2160/0.164kgm^{-3}
μ_g	17.9µPas	17.9µPas	18.6µPas
d_1	0.35µm	0.2µm	0.15µm
I	15000	5000	4000
d_I	8.63µm	3.42µm	2.38µm
V	2m/s	2m/s	2m/s

Because of the uncertainty in the sound pressure level of the transducer, the velocity amplitude is chosen to be 2.0m/s which correspond to 149dB for air and 144dB for helium. The model shows that a small increase in residence time has an effect equal to a similar increase in the velocity amplitude.

The results of the measurements and the modeling will be judged on the following qualitative points:

- Is the initial particle size distribution well represented by the Log-Normal fit? Is an extrapolation justified?
- Are the consecutive measurements consistent?
- Is it possible to conclude from the measurements that coagulation took place?
- How comparable is the shift in particle size distribution between the model and the measurement.

And some quantitative points:

- Did the amount of particles decrease which would be expected if coagulation takes place.
- Is there a change in particle mass concentration and if so can that be explained by other observations or reasoning?
- What sound pressure level should be used in the model to achieve the best possible match between the measurement and the model?

5.2.1. Series 1: Oily particles in instrument air

The input particle size distribution shown in Figure 5-3 is not very well described with the fit of a log-normal distribution, but this is not necessary because the size range is well within the specifications of the OPC and the extrapolation is thus not needed for the modeling.

From the experimental result a particle concentration reduction can be seen for particle sizes below 5µm and an increase in the region of 5-8µm. Unexpected is a decrease in particles for a size larger than 8µm. A visible effect of, the ultrasonic treatment can be seen in Figure 5-2 in which the oil fog becomes more transparent within seconds from turning on the acoustic field. This decrease in opacity suggests that the total amount of droplet area decreases which could be due to increase in droplet size or deposition of the droplets inside the chamber.

From the tabulated result it can be concluded that the particle count decreases by 18% with the ultrasound turned on. However a reduction of volume concentration of 9% suggests also that deposition at the inside of the chamber is enhanced by the acoustic field.

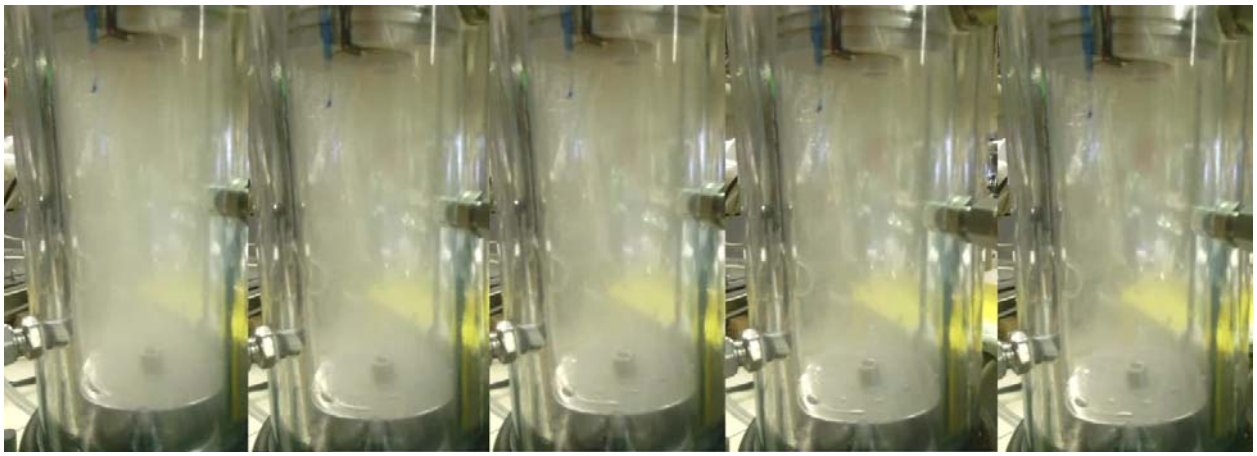

Figure 5-2: Difference in opacity of the aerosol in the coagulation chamber when turning on the ultrasonic transducer, from left to right the time the ultrasound was on: off, after 1s, after 2s,after 4s, after 6s. Also note the oil deposition on the radiation plate of the transducer.

Table 5-2: Results of individual measurements for series 1 which and its averages which. The average of the measurements without treatment is used as in input size distribution for the model and the average measurement of the particle size distribution with treatment is used as a comparison for the model outcome. The measurements which are labeled US are measurements with ultrasonic treatment on and the measurements with the label NO_US are without ultrasonic treatment.

#	Date and time	Count [10^{10}p/m^3]	Concentration [g/m^3]
US120	13-Mar-2013 19:04:57	9.60	2. 63
US121	13-Mar-2013 19:06:24	9.87	2.73
US122	13-Mar-2013 19:07:52	9.97	2.85
US123	13-Mar-2013 19:09:28	10.04	2.88
NO_US124	13-Mar-2013 19:11:21	11.58	2.67
NO_US125	13-Mar-2013 19:12:57	11.80	2.81
NO_US126	13-Mar-2013 19:14:26	12.29	3.32
US129	13-Mar-2013 19:25:20	9.27	2.75
Average no treatment		11.89	2.94
Average with treatment		9.75	2.77

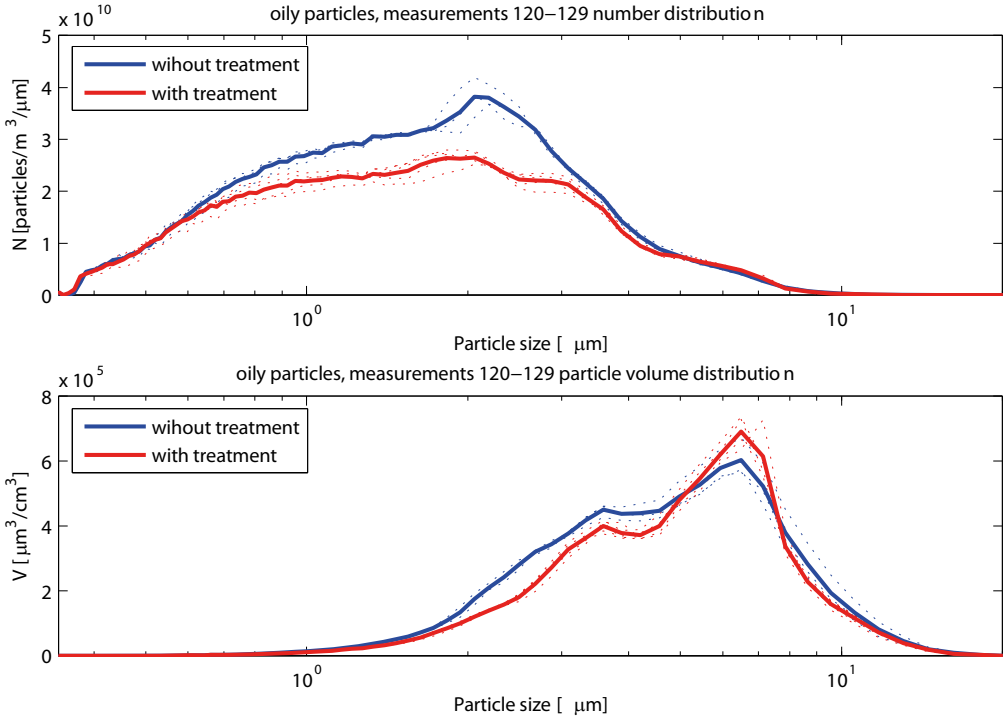

Figure 5-3: A plot of the particle size distributions which are listed in Table 5-2. The dashed lines are the individual measurements and the thick lines are the averages.

The computer model does not take deposition of particles into account and is in general not a very accurate description of the process for this series, it also overestimates the coagulation. In one second of treatment time more coagulation is accomplished than in the measurements 22 seconds.

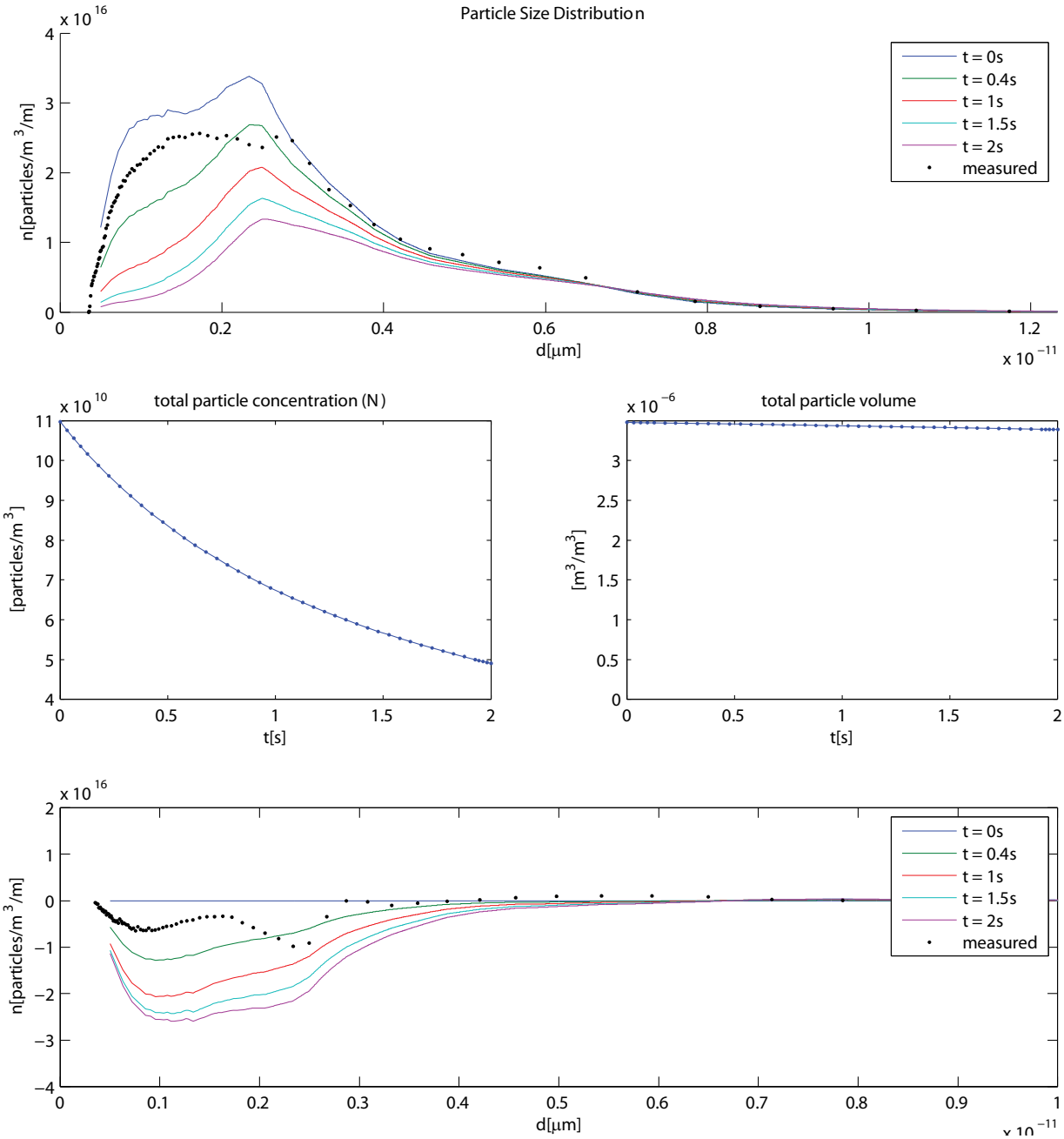

Figure 5-4: Comparison of the model at different time steps and the measured data which corresponds to the solid blue line in Figure 5-3. The third graph shows a decrease in the total particle volume, this is due to the fact that particles agglomerated to a class size outside the modeling domain and its function is thus only to verify if the modeling domain chosen is large enough. Note that the measured residence time is 22s, which is an order of magnitude higher than modeled here.

5.2.2. Series 2: NaCl particles in instrument air

In the second experiment series, the initial particle size distribution is very well represented by a log-normal distribution and this fit is suitable as an extrapolation of the initial particle concentration at the size range outside the measurement range of the OPC.

Figure 5-5 clearly indicates coagulation, because the concentration of particles below 0.7µm decreases and vice versa and particles tend to caogulate up to sizes of 10µm. From Table 5-3 it shows that the particle count decreases with 33%, but the measured mass concentration more than doubles which is not realistic. A reason for this could be that the measured particles are agglomerates which deviate from the spherical form and are overestimated. The volume of the very large particles is especially exaggerated because the mass to diameter ratio scales with the power of three for spherical particles and less for agglomerates[73].

Table 5-3: comparison of consecutive measurements with (US) or without (NO_US) ultrasound treatment enabled.

#	Date and time	Count [10^{10}p/m^3]	Concentration [g/m^3]
NO_US186	14-Mar-2013 13:19:28	6.14	0.032
NO_US187	14-Mar-2013 13:20:57	5.92	0.035
NO_US188	14-Mar-2013 13:22:49	5.76	0.035
NO_US189	14-Mar-2013 13:24:14	5.76	0.030
US190	14-Mar-2013 13:28:11	4.11	0.106
US191	14-Mar-2013 13:29:33	4.15	0.082
US192	14-Mar-2013 13:30:51	4.15	0.057
US193	14-Mar-2013 13:32:12	4.54	0.062
US194	14-Mar-2013 13:36:58	3.53	0.036
US195	14-Mar-2013 13:38:33	3.38	0.045
US197	14-Mar-2013 13:40:08	3.55	0.045
US198	14-Mar-2013 13:41:58	3.65	0.034
NO_US200	14-Mar-2013 13:45:17	5.41	0.010
NO_US201	14-Mar-2013 13:47:23	5.82	0.013
NO_US202	14-Mar-2013 13:49:54	5.80	0.013
Average without treatment		5.80	0.024
Average with treatment		3.88	0.058

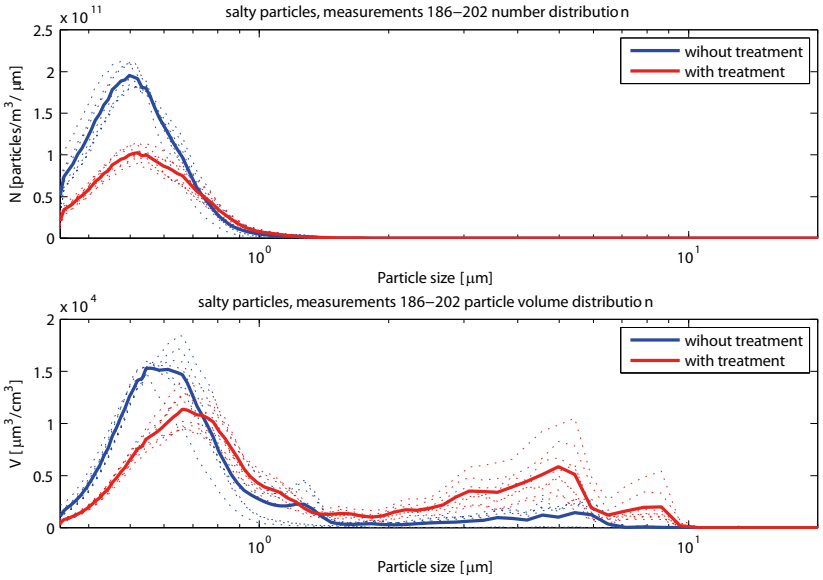

Figure 5-5: 15 Measurements from the OPC for measurement 2 in which the dashed lines represent individual measurements and the solid lines represent the averages for with or without ultrasonic treatment.

The model is a good representation of the measurement which can be seen in Figure 5-6, but the treatment time in the model is twice as long. This however can be mitigated by doubling the velocity amplitude in the model to 4.0 m/s which corresponds to a sound pressure level of over 155dB.

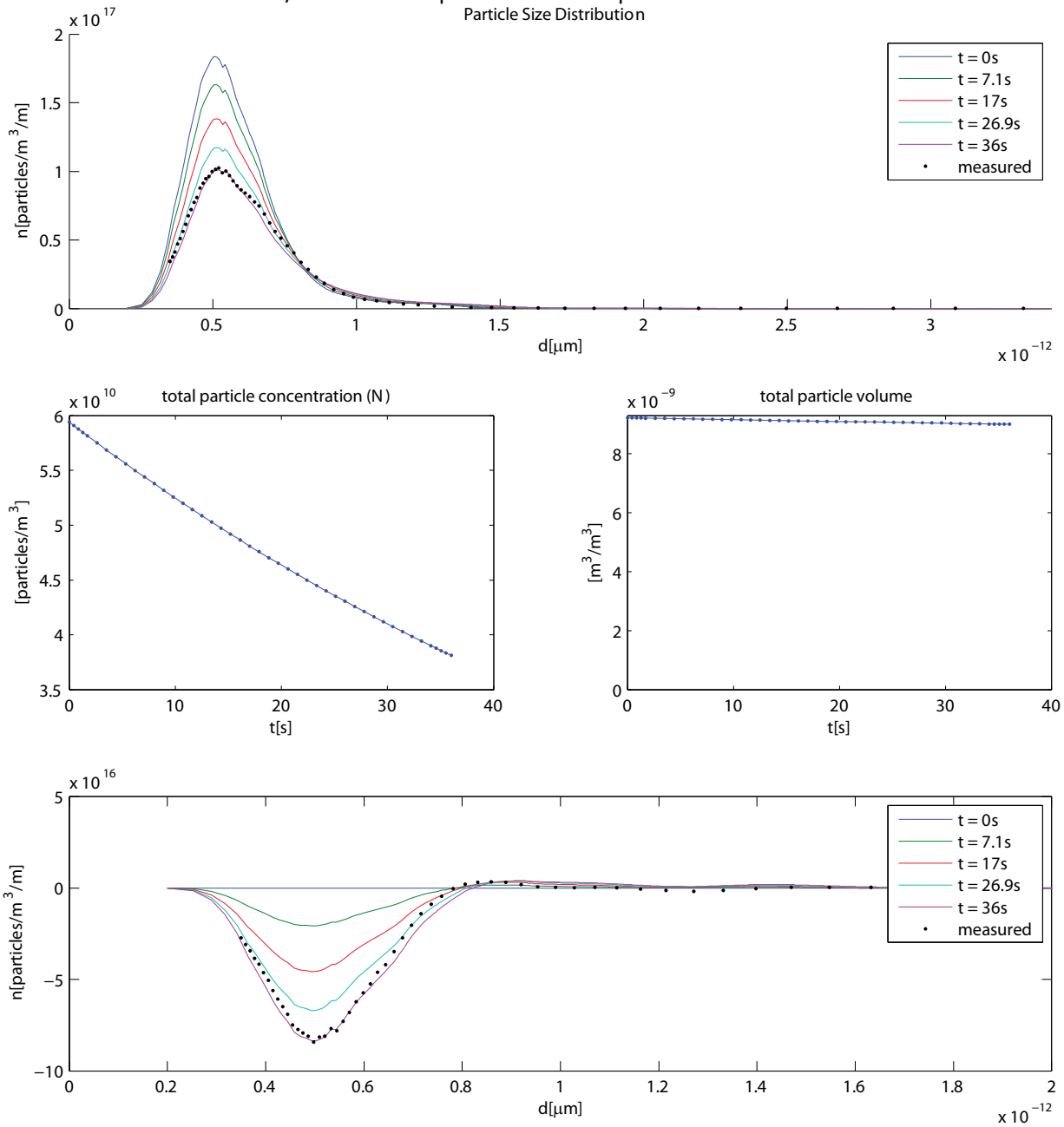

Figure 5-6: Result of the model compared to the measurement of experiment 2: Salty particles in air. The measured residence time is 18s, so the model underestimates the coagulation by half.

5.2.3. Series 3: NaCl particles in helium

In the final experiment series, the atomizer was running on helium instead of in air. Helium has a similar viscosity as air, but a much lower density. The flow through the atomizer is also higher at the

same pressure. This reduces the residence time and the particle concentration in the coagulation chamber which can be seen in Table 5-4 and Figure 5-7.

There is no significant decrease in particle count measured which could be because in the initial distribution an amount of particles are outside the measurement range of the OPC which could be measured after coagulation. This explanation is supported by the measured increase in particle concentration.

Table 5-4: comparison of consecutive measurements with (US) or without (NO_US) ultrasound treatment enabled.

#	Date and time	Count [10^{10}p/m^3]	Concentration [g/m^3]
NO_US215	14-Mar-2013 14:46:49	2.48	0.0041
NO_US216	14-Mar-2013 14:48:27	2.53	0.0041
NO_US217	14-Mar-2013 14:49:55	2.59	0.0041
NO_US218	14-Mar-2013 14:51:18	2.63	0.0041
US221	14-Mar-2013 14:57:33	2.57	0.0048
US222	14-Mar-2013 14:59:01	2.58	0.0048
US223	14-Mar-2013 15:00:21	2.52	0.0045
NO_US224	14-Mar-2013 15:02:00	2.60	0,0040
NO_US225	14-Mar-2013 15:03:38	2.56	0.0039
Average without treatment		2.57	0.0041
Average with treatment		2.56	0.0047

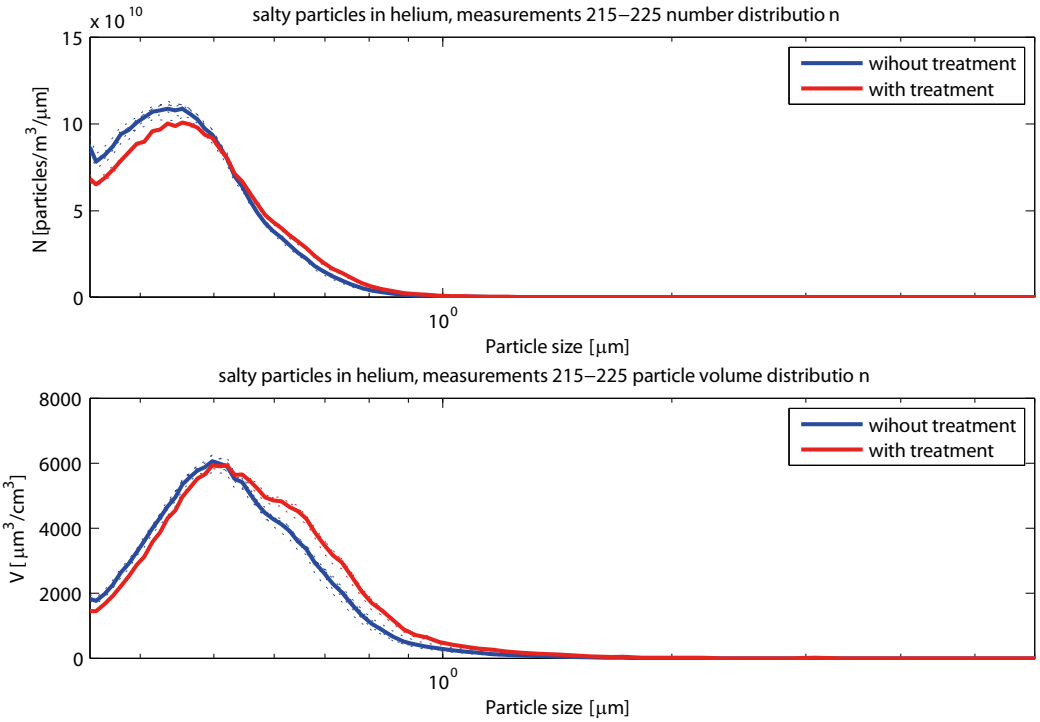

Figure 5-7: Measurements from the OPC for measurement 2 in which the dashed lines represent individual measurements and the solid lines represent the averages for with or without ultrasonic treatment

For this case the model is reasonable description, a decrease in smaller particles and an increase in larger particles. However the model overestimates the particle size. The rate of coagulation is underestimated. To get to similar values the velocity amplitude should be increased to 8m/s which is >156dB.

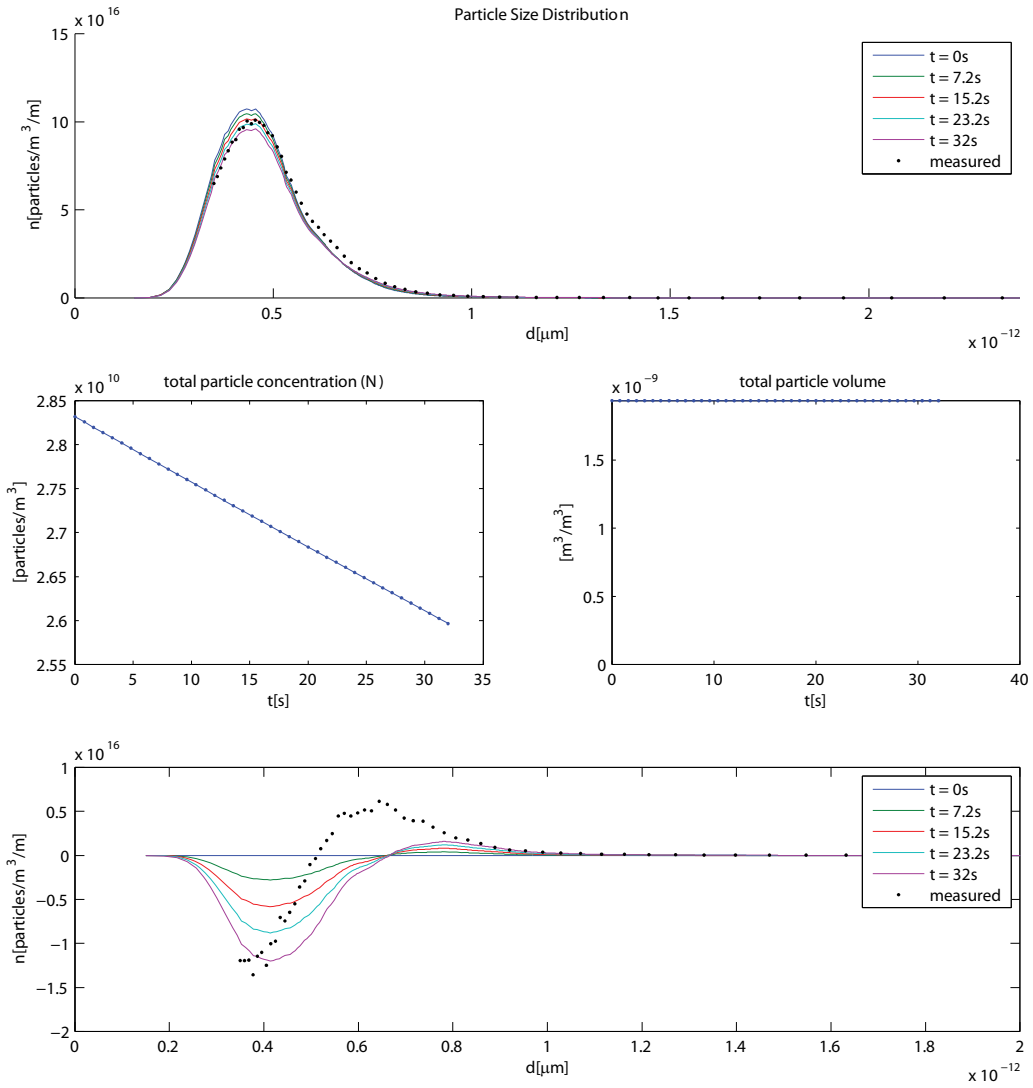

Figure 5-8: Modeling result of the third experiment.

5.3. General observations

Besides the coagulation of aerosols, some general physical observations were made. While running the first experiments with the oily particles, the mode shape of the radiation plate was clearly recognized by ring-formed deposition on the nodes of the plate:

Figure 5-9: Ring shaped deposition on the radiation plate while the transducer was turned off (left) and on (right). The shape of the radiation plate appears to be deform due to the optical properties of the agglomeration chamber.

Another physical phenomenon encountered while running the first experiments is acoustic levitation in which an oil droplet 'hovered' above the radiation plate. Acoustic levitation is a direct effect of the acoustic radiation force[74].

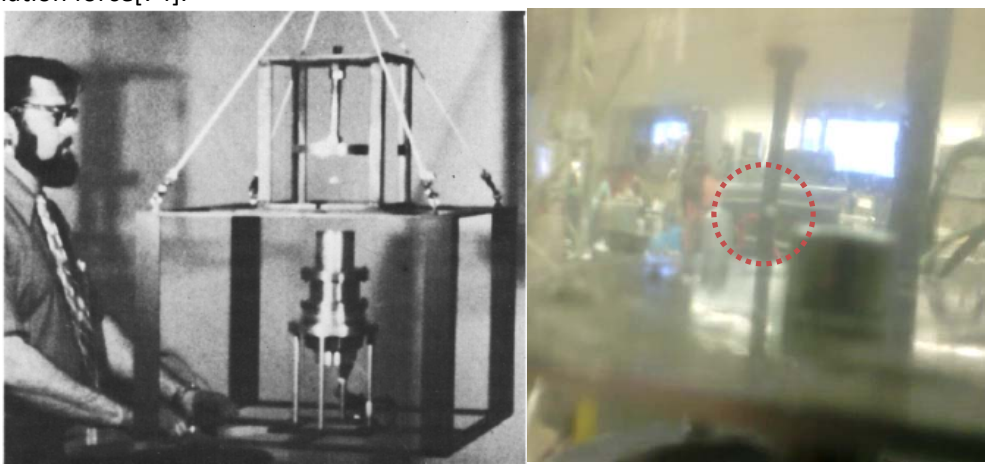

Figure 5-10: Acoustic levitation, left: pioneered in the 1970s[75], right: unintentionally observed in this thesis.

From the modeling the influences of the orthokinetic and acoustic wake effect can be plotted which is done in Figure 5-11. For the orthokinetic kernel the diagonal axis is zero, because particles of the same size have no relative velocity according to this mechanism. For the acoustic wake mechanism the size of the particle is important so its influence is irrelevant for sub-micron particles in regard to the orthokinetic effect. For particles larger than 6µm, the acoustic wake effect becomes the dominant mechanism (Figure 5-11). This advocates the idea of introducing big 'collector' particles to clear up the smaller particles.

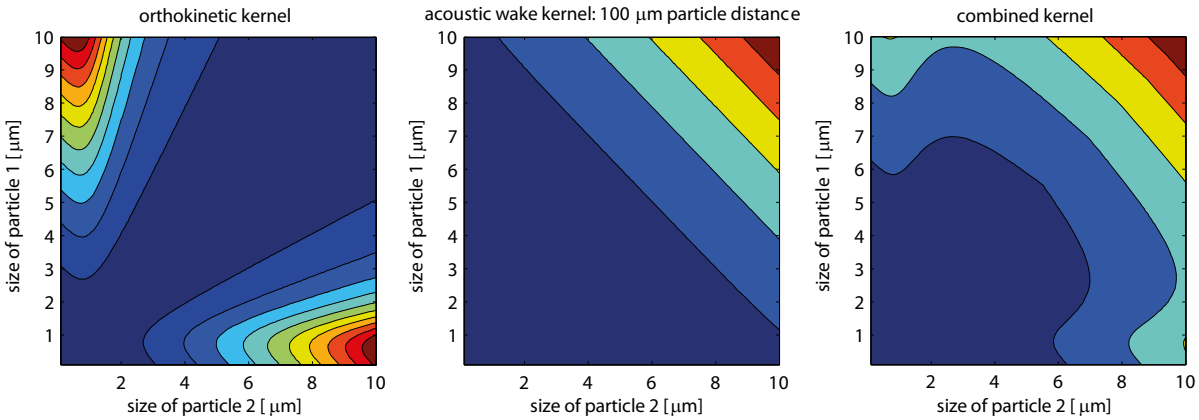

Figure 5-11: Plot of the influence of the orthokinetic mechanism and the acoustic wake kernel. The color of the graph represents the kernel entry and is thus defined as the frequency of two particles engage in a collision for which dark blue represents a low collision frequency and dark red represents a high collision frequency.

5.4. Comparison with result from earlier experiments

Some of the selected measurements from Table 1-1 show similarity with the work done in this thesis. The best comparison can be done with the measurements from Gallego-Juárez et al. from 1999 in which a particle count reduction of 40% was achieved with 2-3 seconds treatment time. Judging from the other papers published from this author regarding the development of ultrasonic transducers since the 1970s[25], it can be speculated that the sound pressure level in his work is at least 170dB (22m/s).

The results of the model suggest that an increase in sound pressure level has the same effect as the same increase in residence time. In the case from Gallego-Juárez et al. 170dB/2-3s would compare with 150dB/20-30 seconds. Comparing this with experiment 2, in which a particle count decrease of 33% was observed, it can be carefully concluded that both results are in the same order of magnitude. Comparison with other work is rather unfruitful because of differences in size distribution, concentration of aerosol, aerosol size, and difference in frequency.

6. Conclusion and recommendations

6.1. Conclusion

The main question of this thesis is:

What are the mechanisms of acoustic coagulation of aerosols?

This was divided into four sub questions:

Which physical effects are of major influence of acoustic coagulation?

In this work the orthokinetic particle interaction and the acoustic wake effect were identified as the main coagulation drivers.

From the literature study many possible coagulation mechanisms were found, from Brownian motion to gravity. Two of those were seen as the main drivers of acoustic coagulation, mainly because of physical evidence, that is the orthokinetic particle interaction and the acoustic wake effect. For both effects physical evidence is presented in previous work (see: Figure 2-2 and Figure 2-1). Both effects result in the effect that the coagulation takes place in a cylindrical shape in the direction of the acoustic wave and will 'sweep' this volume over time. Other physical effects such as acoustic radiation and turbulence 'refill' this mechanism.

The question is on how much each effect contributes to the coagulation rate. From the kernel model it becomes clear (see: Figure 5-11) that the orthokinetic effect is relevant for large size differences. The acoustic wake effect is relevant for larger particles in general.

How do the properties of the gas and the aerosols influence the process?

An influence of particle size, concentration and density of the gas and aerosol was observed, however not with ceteris paribus conditions

A significant decrease in particle concentration due to the acoustic field was observed in experiment series 2, while a less impressive result was obtained from the other two experiments. The difference with experiment series 1 is the particle size and phase. The particles in experiment 2 are almost three times smaller if the log-normal mode is taken as a way of classifying the size of a distribution in one parameter. This suggests that the used 41.8kHz is better at coagulating sub-micron particles than it is at coagulating super-micron particles. The relation between particle size and optimal coagulation frequency are nothing new however[22, 38]. Another possible explanation can be found in the fact that the particles are in the liquid phase. One option is that the coagulated droplets coagulated to a size in which they deposited. Another option is that the pressure fluctuations of the acoustic wave caused a evaporation and condensation of the droplets, in which smaller primary droplets could be created.

The comparison of experiment series 2 with experiment series 3 shows that the latter has a lower particle concentration from which almost none of the particles are bigger than 1µm, this could be of a disadvantage regarding the orthokinetic particle interaction. The biggest difference in helium and air is the density which should not have an influence on the particle entrainment ratio (equation (2.13)). The

acoustic wake effect will also have no major influence in this experiment series because of the high distance between the particles and the lack of particles with a big size.

What is the influence of sound pressure level and residence time?

An increase of the sound pressure level and residence time will lead to an increase in the coagulation.

There is one other comparison between experiment 2 and 3. The residence time of the aerosol is about halved in experiment 3 in comparison with experiment 2. From the model it appears that an increase in residence time equivalates with the same increase in sound pressure level. This is an interesting result for the design of an application based on the suggested technology, however the effect of agglomerate break up still has to be investigated.

Can a population based model be validated by a by a low cost small scale setup?

Looking on the result for experiment 2 the answer would be yes, however if the other experiments are taken into account than it is clearly the case that something is missing.

Especially for experiment 1 it fails to match the measurement results. A possible explanation could be that the temporal pressure fluctuations evaporate and condensate part of the droplets which limits the growth of the droplets and supplies a continue amount of primary droplets. Also the deposition is probably to happen more likely to larger droplets and it is possible that the agglomerates never reach the OPC. However there is no evidence to support these theories.

For experiment three, the induced coagulation is only minor, so changes in the particle size distribution are more difficult to obtain from the measurement errors.

6.2. Recommendations regarding to the modeling approach

- In this work, it is assumed that the particles are spherical, even after agglomeration. A more realistic model would be to assume that the particles are agglomerates consisting of an integer amount of primary particles with the following characteristic radius

$$N = \left(\frac{d_{agglomerate}}{d_{primary}} \right)^{D_f} \tag{6.1}$$

  If the agglomerates are spherical such as is assumed in this model the fractal dimension is 3. However for Brownian agglomerates this value is in the range of 1.6-2.2[73]. This equation could be used for a population model in which the size bins are expressed in an primary particle count instead of particle volume, if a relation can be found between the optical diameter of agglomerates and the count of primary particles in the agglomerate, the measurement error of the OPC can also be taken into account of the model.
- The modeling algorithm used in this thesis has some inefficiency. The kernel is by definition a symmetric matrix which means it takes almost twice the amount of memory as is necessary, also the model loop in the 'creation' part is not taking advantage of the symmetry.
- For modeling a continues system a steady state model could be derived, the following mass balance should be worked out:

$$\underbrace{\frac{dn}{dt}}_{=0} = input + creation - destruction - output \tag{6.2}$$

6.3. Recommendations regarding to the practical approach

- For these kind of ultrasonic transducers, greater than 80% electroacoustic efficiency is possible[76] so in this setup 162dB should be possible, assuming that the transducer is taking up 60W of electrical power as it is specified, this means that further harmonizing the resonance frequencies of the horn, transducer and radiation plate will further increase the sound pressure level of the transducer assembly.
- The optical particle counter (OPC) could be combined with a differential mobility analyzer (DMA) or other instrument to determine the particle size distribution
- Instead of measuring the pressure with a piezo-electric pressure sensor, a hot wire anemometer can be used to measure the velocity amplitude of the acoustic wave.
- By combining two aerosol sources, a bidisperse aerosol could be created.

Acknowledgements

Since a lot of people helped me with this thesis, for which I owe them many thanks.

For both giving me the idea to use the Smoluchowski modeling approach and to make use of the equipment in the nanoparticle lab at the chemical engineering faculty I owe much thanks to Konstantinos Barmpounis who also took the time to help me with my thesis numerous times.

From the geoscience and engineering department of the civil engineering faculty great thanks go out to Karel Heller, who lent me his literally irreplaceable RF amplifier and came to the rescue when the power gauge went crazy because of improper cable shielding. He also granted me access to his component analyzer for measuring the impedance of the transducer.

For the work on the ultrasonic transducer design I had some help from various people of the precision and micro engineering department of the 3mE faculty. Matthijs Langelaar and Paolo Tiso helped me with the modeling of the transducer and Tjitte-Jelte Peters and Paul van der Valk made it possible for me to use the Laser Doppler Vibrometer. Also to PME student Nick Teunisse made a COMSOL of a stepped plate transducer to create a single phase acoustic field.

Also I would like to thank Henry den Bock from the acoustic imaging department of the TNW-faculty. He arranged for me to use the soundproof room with calibrated microphone to measure the sound pressure level.

And I won't forget to mention my graduation committee prof. B.J. Boersma, Dr.ir.W. de Jong, Dr.Ir.P.Plaza and as mentioned before Dr.ir.M. Langelaar. It was a very pleasant collaboration with Wiebren and Piotr and I got a lot of tips and mental support from Joppe Buntsma, who did his master thesis on the same subject.

I learned a lot from doing this project and I especially enjoyed the cooperation which I got from all over the university.

Thank you!

Andries van Wijhe

Appendix A: Overview of formulations for particle drag force and particle entrainment ratio

A lot is known about the movement of spherical particles in a flow. The first mathematical description of a particle in a sound field dates back to 1891 from Walter König[77] in which he starts with assuming non-viscous flow[21] :

$$F = \frac{d}{dt}\left(u - v\right) = \underbrace{m'\frac{du}{dt}}_{\substack{\text{reaction of the medium}\\ \text{due to pressure difference}}} - \underbrace{\frac{m'}{2}\left(\frac{du}{dt} - \frac{dv}{dt}\right)}_{\text{acceleration of the particle with respect to the medium}} \tag{A.1}$$

In which m' is the mass displaced by the particle, with the viscous forces added:

$$m\frac{du}{dt} = \frac{3}{2}m'\frac{dv}{dt} - \frac{1}{2}m'\frac{du}{dt} - \frac{9}{4}m'\omega\beta\left(1+\beta\right)\left(u - v\right) - \frac{9}{4}m'\beta\left(\frac{du}{dt} - \frac{dv}{dt}\right)^{2} \tag{A.2}$$

with:

$$\beta = \frac{2}{d}\sqrt{\frac{2\mu}{\omega\rho_f}} \tag{A.3}$$

Resulting β>22 for 40kHz in air for a 1 micron particle, which means that $\beta^2 \approx \beta\left(1+\beta\right)$:

$$\frac{m}{m'}\frac{du}{dt} = \frac{3}{2}\frac{dv}{dt} - \frac{1}{2}\frac{du}{dt} - \frac{9}{4}\omega\beta^2\left(u - v\right) - \frac{9}{4}\beta\left(\frac{du}{dt} - \frac{dv}{dt}\right) \tag{A.4}$$

This can be solved into an entrainment ratio of the particle in the gas:

$$q = \sqrt{\frac{1 + 3\beta + \frac{9}{2}\beta^2 + \frac{9}{2}\beta^3 + \frac{9}{4}\beta^4}{\alpha^2 + 3\alpha\beta + \frac{9}{2}\beta^2 + \frac{9}{2}\beta^3 + \frac{9}{4}\beta^4}} \tag{A.5}$$

and a phase difference of:

$$\tan\left(\varphi - \theta\right) = \frac{\frac{3}{2}\left(\alpha - 1\right)\beta\left(1+\beta\right)}{\alpha\left(1 + \frac{3}{2}\beta\right) + \frac{3}{2}\beta + \frac{3}{2}\beta^2 + \frac{3}{2}\beta^3 + \frac{3}{2}\beta^4} \tag{A.6}$$

with:

$$\alpha = \frac{2m}{3m'} = \frac{2\rho_p}{3\rho_f} \tag{A.7}$$

Other particle drag force equations are based on stokes flow [34, 35](A.8) and its entrainment ratio (BFH) [21, 22, 39](A.9). The particle drag force based on Oseen's flow is described by equation (A.10)[34, 36], for which the entrainment ratio is described with equation (A.11)[40]. A further Taylor expansion of the particle drag force was done by Chester and Breach Particle (A.12)[37]. The most extensive entrainment ratio formulation was done by Temkin and is based on the Basset-Boussinesq-Oseen equation[41, 78] for which the modulus equals to the entrainment ratio and the argument to the phase delay[47](A.13).

$$F_{drag} = 3\pi\mu\left(u - v\right)d \tag{A.8}$$

[2] This reduces to Stokes drag force if the flow field is steady state.

$$q = \frac{1}{\sqrt{1+\omega^2\tau^2}} \qquad \tan\left(\varphi-\theta\right) = \omega\tau \tag{A.9}$$

$$F_{drag} = 3\pi\mu\left(u-v\right)d\left(1+\frac{3}{16}d\rho\frac{\left(u-v\right)}{\mu}\right) \tag{A.10}$$

$$q = \frac{1}{\sqrt{1+\left(\omega\tau\Big/1+\frac{3}{8}\mathrm{Re}\right)^2}} \tag{A.11}$$

$$F_{drag} = 3\pi\mu\left(u-v\right)d\left(1+\frac{3}{8}\mathrm{Re}+\frac{9}{40}\mathrm{Re}^2\left(\log\mathrm{Re}+e+\frac{5}{3}\log 2+\frac{232}{360}\right)\right) \tag{A.12}$$

$$Q = \frac{1+\frac{3}{2}\sqrt{\omega\tau\delta}-i\frac{3}{2}\left(\delta\omega\tau+\sqrt{\omega\tau\delta}\right)}{1+\frac{3}{2}\sqrt{\omega\tau\delta}-i\left(\omega\tau\left(1+\frac{\delta}{2}\right)+\frac{3}{2}\sqrt{\omega\tau\delta}\right)} \qquad q = \left|Q\right| \quad \tan\phi = \frac{\mathrm{Im}\left(Q\right)}{\mathrm{Re}\left(Q\right)} \tag{A.13}$$

with $\delta = \dfrac{\rho_p}{\rho_f}$

Appendix B: Sound pressure/velocity/intensity calculations

Sound 'volume' or intensity can be defined in various units such which are related to velocity or pressure amplitude or radiated power. For a monochromatic sound wave, the following three expressions for the same sound wave can apply[22]:

$$\begin{aligned} y &= y_0 \sin \omega t \\ v &= v_0 \cos \omega t \\ p &= p_0 \cos \omega t \end{aligned} \tag{B.1}$$

The relation between pressure and velocity is governed by the acoustic impedance z. The displacement amplitude is easily obtained by integrating the velocity amplitude:

$$\begin{aligned} z &= \rho_f c_f \\ v_o &= \frac{p_{rms}}{Z}\sqrt{2} \\ y_0 &= \frac{v_0}{f} \end{aligned} \tag{B.2}$$

The radiated power or intensity is defined as[22]:

$$J = \frac{p_{rms}^2}{\rho_f c_f} \tag{B.3}$$

These units can be converted to a logarithmic unit as in the sound pressure level (SPL) using a reference which is the audible threshold for the human ear.

$$SPL = 20 \log_{10} \frac{p_{rms}}{p_r} \tag{B.4}$$

In which the reference in intensity is set to 10^{-12}W/m^2[33]. The physical relations of sound waves in air $c = 343.8\, m/s$, $\rho = 1.2\, kg/m^3$ and $\gamma = 1.4$ the properties at 41.8kHz and 101.325kPa atmospheric pressure:

AIR	140dB	150dB	160dB
Intensity	97W/m^2	970 W/m^2	9695 W/m^2
Pressure amplitude (RMS)	200Pa	632Pa	2 000Pa
%of atmospheric pressure	0.2%	0.6%	2.0%
Velocity amplitude	0.69m/s	2.16m/s	6.86m/s
% of speed of sound	0.2%	0.6%	2.0%
Amplitude	16µm	52µm	164µm
% of wavelength	0.2%	0.6%	2.0%

The same table can be made for helium at the same conditions $c = 991.1\, m/s$, $\rho = 0.17\, kg/m^3$ and $\gamma = 1.67$:

He	140dB	150dB	160dB
Intensity	241W/m^2	2 408 W/m^2	24 083 W/m^2
Pressure amplitude (RMS)	200Pa	632Pa	2 000Pa
%of atmospheric pressure	0.2%	0.6%	2.0%
Velocity amplitude	1.2m/s	3.8m/s	12.04m/s
% of speed of sound	0.12%	0.38%	1.19%
Amplitude	29µm	91µm	288µm
% of wavelength	0.01%	0.04%	0.12%

Appendix C: Derivation of the Smoluchowski equation

The general equation for each bin is:

$$\frac{\partial n_i(x,t)}{\partial t} = creation - destruction \tag{C.1}$$

The equation can be worked out for a model containing 5 bins and can then be expanded to generalize it to I bins. Take the coagulation kernel K:

$$K = \begin{pmatrix} K_{1,1} & K_{1,2} & K_{1,3} & K_{1,4} & K_{1,5} \\ K_{1,2} & K_{2,2} & K_{2,3} & K_{2,4} & K_{2,5} \\ K_{1,3} & K_{2,3} & K_{3,3} & K_{3,4} & K_{3,5} \\ K_{1,4} & K_{2,4} & K_{3,4} & K_{4,4} & K_{4,5} \\ K_{1,5} & K_{2,5} & K_{3,5} & K_{4,5} & K_{5,5} \end{pmatrix} \tag{C.2}$$

The differential equation for the first bin is:

$$\begin{aligned} \frac{\partial n_1}{\partial t} &= -K_{1,1}n_1n_1 - K_{1,2}n_1n_2 - K_{1,3}n_1n_3 - K_{1,4}n_1n_4 - K_{1,5}n_1n_5 \\ &= -n_1\left(K_{1,1}n_1 + K_{1,2}n_2 + K_{1,3}n_3 + K_{1,4}n_4 + K_{1,5}n_5\right) \\ &= -n_1\sum_{j=1}^{5} K_{1,j}n_j \end{aligned} \tag{C.3}$$

and for the second bin:

$$\frac{\partial n_2}{\partial t} = K_{1,1}n_1n_1 - n_2\sum_{j=1}^{5} K_{2,j}n_j \tag{C.4}$$

and for the fifth:

$$\begin{aligned} \frac{\partial n_5}{\partial t} &= K_{1,4}n_1n_4 + K_{2,3}n_2n_3 - n_5\sum_{j=1}^{5} K_{5,j}n_j \\ &= \frac{1}{2}\sum_{i+j=5}^{5} K_{i,j}n_in_j - n_5\sum_{j=1}^{5} K_{5,j}n_j \\ &= \frac{1}{2}\sum_{j=1}^{4} K_{5-j,j}n_jn_{5-j} - n_5\sum_{j=1}^{5} K_{5,j}n_j \end{aligned} \tag{C.5}$$

Note that the addition of the 1/2 in equation (C.5) is due to the fact that in the model the particle is created twice. With some reasoning this can be generalized to bin i in a model with I bins:

$$\frac{\partial n_i}{\partial t} = \underbrace{\frac{1}{2}\sum_{j=1}^{i-1} K_{i-j,j}n_jn_{i-j}}_{creation} - \underbrace{n_i\sum_{j=1}^{I} K_{i,j}n_j}_{destruction} \tag{C.6}$$

This is known as the Smoluchowski equation[49].

Appendix D: OPC data handling

The raw data gathered from the OPC consists of a particle size range and a integer particle count. To fill in the rest of the data, a measurement time and volume, and time/date stamp are also supplied. With this the particle size and volume distribution can be obtained.

The average bin size and volume are derived from the calibration of the machine with spherical sample particles, note that another method of calculating the average volume is use the average diameter to calculate the volume instead of calculate the average of two volumes. Another error might by induced is that by calculating the volume the particles are assumed to be spherical.

$$\begin{aligned} d &= \frac{d_{\min} + d_{\max}}{2} \\ V &= \frac{V_{\min} + V_{\max}}{2} = \left(d_{\min}^3 + d_{\max}^3\right)\frac{\pi}{12} \end{aligned} \tag{D.1}$$

As the data is now, the amount of size in a bin is dependent on the width of the bin which is undesirable, since the width of the bin is irrelevant of the determination of the particle size distribution. Therefore, the count and volume are divided by the width of the bin:

$$\begin{aligned} n_i &= \frac{N_i}{\left(d_{\max} - d_{\min}\right)V_{OPC}}corr \\ v_i &= \frac{V_i}{\left(d_{\max} - d_{\min}\right)V_{OPC}}corr \\ corr &= \begin{cases} \dfrac{\phi_{OPC}}{\phi_{atomizer}} & if \phi_{OPC} > \phi_{atomizer} \\ 1 & else \end{cases} \end{aligned} \tag{D.2}$$

The diameter classification of non-spherical particles is ambiguous, in this work, the particle diameter is determined by the volume and the assumption that it is spherical. Other diameter classification which are relevant for this work are:

- Stokes Diameter (Aerodynamic equivalent): The diameter of a spherical particle which has the same settling velocity as a the described arbitrary shaped particle. For granule, disk or cubes this approximation is correct within 10%, but for particles which have a particle in which the size in one dimension dominates such as a fiber or even a thin flake the error can go up to 200%.[59]
- Optical equivalent diameter, the diameter which is measured by optical particle counters. This strongly depends on the order of magnitude of the size which is shown in Figure 4-2. The region of interest for this thesis is the Mie-region.

Appendix E: MATLAB model

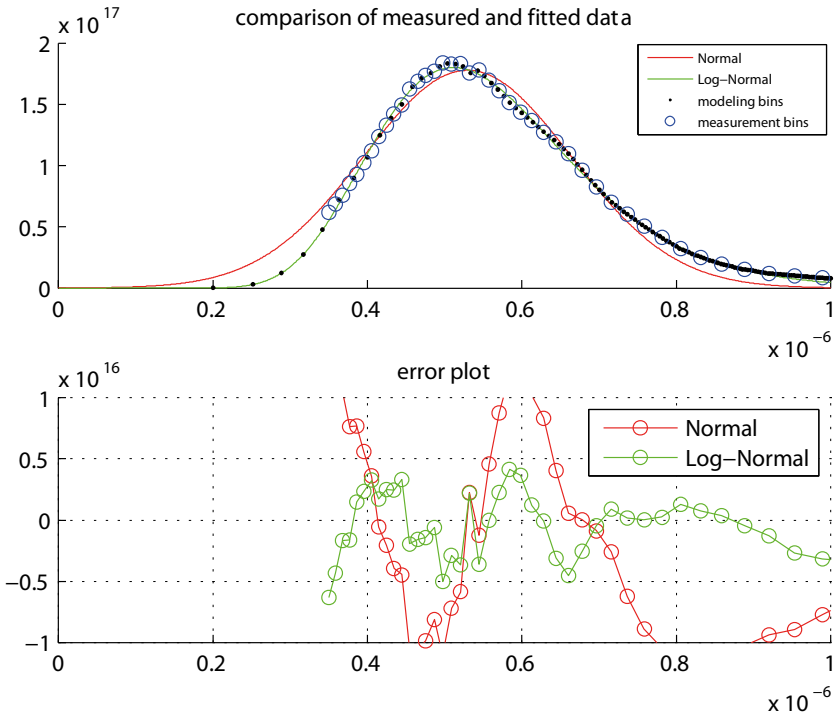

Figure E-2: Distribution fit of experiment 2

The entrainment ratios of the three experiment series are:

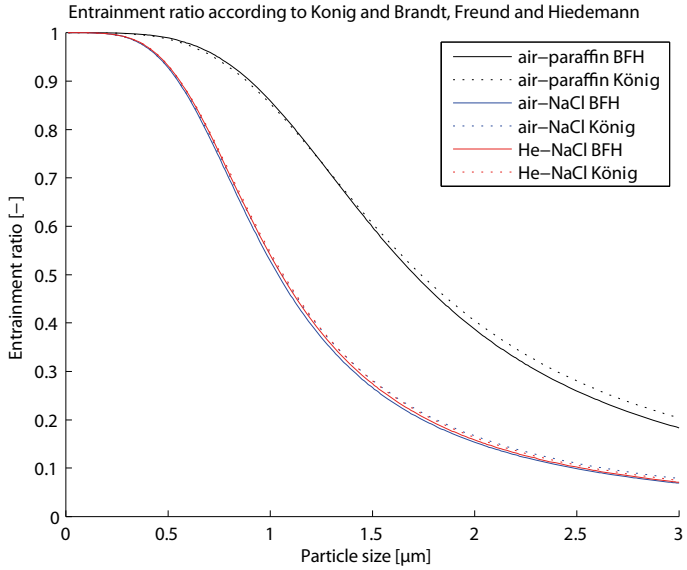

Figure E-3: Entrainment ratio for the three discussed cases calculated with different methods.

MATLAB M-files:

Model_driver.m:

```
%%%%%%%%%%%%%%%%%%%%%%%%%%%%%%%%%%%%%%%%%%%%%%%%%%%%%%%%%%%%%%%%%%%%%%%%%%%%%%%%
%% Model_driver.m                                                               %%
%% Main script kernel model for acoustic coagulation of aerosols               %%
%% All the parameters are in SI units!                                          %%
%% Andries van Wijhe 2013                                                       %%
%%%%%%%%%%%%%%%%%%%%%%%%%%%%%%%%%%%%%%%%%%%%%%%%%%%%%%%%%%%%%%%%%%%%%%%%%%%%%%%%
clear; clc; warning off;
global K_or Kr_aw t_end

%% Select model properties from subfolder with parameters and input files
rmpath NaCl_He NaCl_air Oil_air
addpath(questdlg('Which experiment?'...
    ,' ','NaCl_He','NaCl_air','Oil_air',' '))

%% Load model/physics parameters from subfolder
tic                     %start timer
parameters              %load parameters from subfolder
init_PSD                %load initial PSD from subfolde

%% Kernel creation
K_or =Orthokinetic_Kernel (d1,I,rho_p,mu_g,V,omega);
Kr_aw = Acoustic_Wake_Kernel(d1,I,rho_p,rho_f, mu_g, V, omega);

%% Display information
display(['initialization time: ',num2str(toc),' s'])
display([num2str(I),' bins, ranging from '...
    ,num2str(d(1)*1e6),' to ',num2str(max(d)*1e6),' micron'])

%% ode solving
tic                                     %restart timer
w = waitbar(0,'ODE Solving...');        %progress bar
[t,n] = ode45(@diff_n,[0 t_end],n0);    %ode solving
close(w);                               %close progress bar
display(['simulation time: ',num2str(toc),' s'])

%% Plot output
plot_output
%%%%%%%%%%%%%%%%%%%%%%%%%%%%%%%%%%%%%%%%%%%%%%%%%%%%%%%%%%%%%%%%%%%%%%%%%%%%%%%%
```

Parameters.m:

```
%%%%%%%%%%%%%%%%%%%%%%%%%%%%%%%%%%%%%%%%%%%%%%%%%%%%%%%%%%%%%%%%%%%%%%%%%%%%%%%%
%% Parameters.m                                                                 %%
%% Loads model specific data                                                    %%
%% Experiment 2: Parameters NaCl - air                                          %%
%%%%%%%%%%%%%%%%%%%%%%%%%%%%%%%%%%%%%%%%%%%%%%%%%%%%%%%%%%%%%%%%%%%%%%%%%%%%%%%%

%d1     [m] smallest particle diameter
%I      [bins] amount of particle size bins
%omega  [rad/s] frequency of sound wave
%tau1   [s] relaxation time of smallest particle

%% Simulation control
```

```
I = 4000;                   %[bins] total amount of bins
t_end = 18;                 %[time] total simulation time
d1 =0.2e-6;                 %[m] particle size in smallest calculation bin
f = 41.88;                  %[kHz] ultrasound frequency
V = 4;                      %[m/s] velocity amplitude of sound wave

%% physical data
rho_p = 2160;               %[kg/m^3]
mu_g = 17.9e-6;             %[Pas]
rho_f = 1.20;               %[kg/m^3]

%% Correction for aerosol dillution
q_in = 1.96;                %[l/min] flow from atomizer
q_T = 3;                    %[l/min] flow from OPC
dil = q_T/q_in;             %[-] multiplication factor for measured PSD

%% Calculations
omega = 1e3*2*pi*f;         %[rad/s]

%% Import dataset of threated aerosols and average
nt_measured{1} = importtopas('US190.grn');
nt_measured{2} = importtopas('US191.grn');
nt_measured{3} = importtopas('US192.grn');
nt_measured{4} = importtopas('US193.grn');
nt_measured{5} = importtopas('US194.grn');
nt_measured{6} = importtopas('US195.grn');
nt_measured{7} = importtopas('US197.grn');
nt_measured{8} = importtopas('US198.grn');
nt_meas_met.d = nt_measured{1}.bin(:,3)*1e-6;
nt_meas_met.n = (nt_measured{1}.n+nt_measured{2}.n+nt_measured{3}.n+...
    nt_measured{4}.n+nt_measured{5}.n+nt_measured{6}.n+nt_measured{7}.n...
    +nt_measured{8}.n)*1e12/8 * dil;
nt_meas_met.v = (nt_measured{1}.v+nt_measured{2}.v+nt_measured{3}.v+...
    nt_measured{4}.v+nt_measured{5}.v+nt_measured{6}.v+nt_measured{7}.v...
    +nt_measured{8}.v)*1e-6/8* dil;
nt_meas_met.n(1) = [];
nt_meas_met.d(1) = [];
nt_meas_met.v(1) = [];

%% Plot end
n_plot = 2e-6;
```

init_PSD.m

```
%%%%%%%%%%%%%%%%%%%%%%%%%%%%%%%%%%%%%%%%%%%%%%%%%%%%%%%%%%%%%%%%%%%%%%%%%%%%%%%
%% init_PSD.m                                                                  %%
%% initializes model specific initial particle size distribution based on%%
%% measurements and extrapolation                                              %%
%% Experiment 2: Parameters NaCl - air                                         %%
%%%%%%%%%%%%%%%%%%%%%%%%%%%%%%%%%%%%%%%%%%%%%%%%%%%%%%%%%%%%%%%%%%%%%%%%%%%%%%%

%% Create initial particle distribution for modeling
close all
subplot 211
hold on
%% Load PSD of untreated aerosols
```

```
PSD_import = importtopas('NO_US186.grn');
PSD_import_2 = importtopas('NO_US187.grn');
PSD_import_3 = importtopas('NO_US188.grn');
PSD_import_4 = importtopas('NO_US189.grn');

%% Take average of measurements and convert to standard SI units
% convert from micron to m
PSD_metric.d = PSD_import.bin(:,3) * 1e-6;                              %[m]
% and from particles/cm^3/micron to particles/m^3/m
PSD_metric.n = dil * 2.5e11 *(PSD_import.n + PSD_import_2.n...
    + PSD_import_3.n +PSD_import_4.n) ;                  %[particles/m^3/m]
PSD_metric.dd = (PSD_import.bin(:,2)-PSD_import.bin(:,1)) * 1e-6; %[m]width
% Ignore first size bin which is erroneous
PSD_metric.d(1) = [];
PSD_metric.n(1) = [];
PSD_metric.dd(1) = [];

%% Measured amount of particles without extrapolation and normalize
N = sum(PSD_metric.n.*PSD_metric.dd);           %[particles] total measured
PSD_norm.n = PSD_metric.n/N;             %[-]pdf of measured area (sum = 1)

%% fit to normal (Gaussian) size distribution
Gauss = @(p,d) (1 ./(p(1) .* (2.*pi).^0.5 ))...             %p = [sigma mu]
    * exp(-((d-p(2)).^2)./2./p(1).^2);
G.p(1) = sum(PSD_metric.d .* PSD_metric.n)/sum(PSD_metric.n);
G.p(2) = (sum((PSD_metric.n .*(G.p(1) -
PSD_metric.d).^2))/sum(PSD_metric.n)).^0.5;
errorGauss = @(N)fitPSD(PSD_metric,N,Gauss,G.p);
[G.N, G.error] = fminbnd(errorGauss,0.1*N,10*N);
[G.error, G.p] = fitPSD(PSD_metric,G.N,Gauss,G.p);
plot(0:1e-9:2e-6,G.N*Gauss(G.p,0:1e-9:2e-6),'r')

%% fit to log-normal  distribution p=[sigma mu]
LogNormal = @(p,d) (1 ./d ./ (2.*pi .* p(1).^2).^0.5 )...   %p = [sigma mu]
    .* exp(-((log(d)-p(2)).^2)./2./(p(1).^2));
LN.p(1) = log(G.p(1));
LN.p(2) = 0.1;
errorLogNormal = @(N)fitPSD(PSD_metric,N,LogNormal,LN.p);
[LN.N, LN.error] = fminbnd(errorLogNormal,0.1*N,10*N);
[LN.error, LN.p] = fitPSD(PSD_metric,LN.N,LogNormal,LN.p);
plot(0:1e-9:2e-6,LN.N*LogNormal(LN.p,0:1e-9:2e-6),'g')

%% Bin distribution creation for model
d = (d1^3 * (1:I)).^(1/3);                              %[m] Bin distribution
dd = (d1^3 * (2:I+1)).^(1/3)-(d1^3 * (1:I)).^(1/3);     %[m] Bin width
dv = d.^3 * pi/6;                                       %[m^3/particle]

%% fill bins with data from either extrapolation or measurement data
for i =1:I
    if PSD_metric.d(1)<d(i) %% if within range
        n0(i) = interp1(PSD_metric.d,PSD_metric.n,d(i)...
            ,'linear','extrap').*dd(i);            %interpolate
    else
        n0(i) = LN.N * LogNormal(LN.p,d(i)) *dd(i); %or estimate
    end
end
```

```
plot(d,n0./dd,'.k')
plot(PSD_metric.d(1:50), PSD_metric.n(1:50),'o')
title('comparison of measured and fitted data')
legend('Normal','Log-Normal','modeling bins','measurement bins')
a = axis; %Resize axis
a(2) = 1e-6;
axis(a)

%% Calculate and plot difference with distribution:
subplot 212
hold on
title('error plot')
G.error = sum(abs(G.N*Gauss(G.p,PSD_metric.d)-PSD_metric.n))...
    /sum(PSD_metric.n)*100;
LN.error = sum(abs(LN.N*LogNormal(LN.p,PSD_metric.d)-PSD_metric.n))...
    /sum(PSD_metric.n)*100;
plot(PSD_metric.d,G.N*Gauss(G.p,PSD_metric.d)-PSD_metric.n,'o-r')
plot(PSD_metric.d,LN.N*LogNormal(LN.p,PSD_metric.d)-PSD_metric.n,'o-g')
grid on
a = axis; %Resize axis
a(2) = 1e-6;
a(3) = -1e16;
a(4) = 1e16;
axis(a)
legend('Normal','Log-Normal')
```

Orthokinetic_Kernel.m

```
function [ K ] = Orthokinetic_Kernel(d1,I,rho_p, mu_g, V, omega)
%Kernel.m Calculation of the coagulation kernel based on the entrainment
%ratio and sound pressure level
%d1     [m] smallest particle diameter
%I      [bins] amount of particle size bins
%omega  [rad/s] frequency of sound wave
%rho_p  [kg/m^3]
%mu_g   [Pas]

%% memory allocation
K = zeros(I);
d = zeros(1,I);
tau = zeros(1,I);
%% creation of array variables
for i=1:I
    d(i) = (d1^3 * i)^(1/3);              %[m] Diameter of particle i
    tau(i) = d(i)^2 * rho_p / 18 / mu_g;  %[s] Relaxation time of particle i
end

%% creation of matrix variables
for i=1:I
    for j=1:I
        CCS = pi/4 * (d(i) + d(j))^2;     %[m^2] Collisional Cross Section
        u_rel = V * 2 / pi *...           %[m/s] averaged relative velocity
            abs(omega * (tau(i) - tau(j)))/...
            sqrt(1+omega^2 * tau(i)^2)/...
            sqrt(1+omega^2 * tau(j)^2);
        K(i,j) = CCS * u_rel;             %[m3/s] Kernel entry
    end
```

```
end
```

Acoustic_Wake_Kernel.m

```
function [ Kr ] = Acoustic_Wake_Kernel(d1,I,rho_p,rho_f, mu_g, V, omega)
%Kernel.m Calculation of the acoustic wake kernel based on Dianov's
% equation
%d1     [m] smallest particle diameter
%I      [bins] amount of particle size bins
%omega  [rad/s] frequency of sound wave
%rho_p  [kg/m^3]
%mu_g   [Pas]

%% memory allocation
Kr = zeros(I);
d = zeros(1,I);
tau = zeros(1,I);
l_st = zeros(1,I);
h = zeros(1,I);
l = zeros(1,I);
%% creation of array variables
for i=1:I
    d(i) = (d1^3 * i)^(1/3);                                          %[m]
    tau(i) = d(i)^2 * rho_p / 18 / mu_g;                              %[s]
    l_st(i) = omega * tau(i) / sqrt(1 + omega^2 * tau(i)^2);          %[-]
    h(i) = 9 * V / pi / omega / d(i) * rho_f/rho_p;                   %[-]
    l(i) = l_st(i)/sqrt(1 + 2*h(i) * l_st(i)^2 + h(i)^2*l_st(i)^4);   %[-]
end

%% creation of matrix variables
for i=1:I
    for j=1:I
        CCS = pi/4 * (d(i) + d(j))^2;                                 %[m^2]
        u_relr = 3/4*V/pi *(d(i) * l(i) + d(j) * l(j));               %[m^2/s]
        Kr(i,j) = CCS * u_relr;                                       %[m4/s]
    end
end
```

fit_PSD.m

```
function [ error,p ] = fitPSD( PSD,N,distribution,p0 )
% Fit PSD to any given distribution:
% corrected distribution for
n = PSD.n/N;

% Fitted values and error.
p = nlinfit(PSD.d,n,distribution,p0);
error = sum(abs(N*distribution(p,PSD.d)-PSD.n))/sum(PSD.n)*100;
end
```

importtopas.m

```
function [ PSD_data ] = importtopas( filename )
%% Import function file for getting TOPAS data in MATLAB with the following
data:
% Total count
```

```
% Concentration
% total particle volume
% measured volume
% measured time
% time and date
% PSD in number and volume

%% Import raw data, the data uses a " " delimiter
rdata = importdata(filename,' ',1);

%% amount of bins
k = (str2num(rdata.textdata{1}));

%% Get data from bins
% Total particle volume
PSD_data.V = 0;
for i = 1:k
    %% Bin size
    PSD_data.bin(k-i+1,:) = [rdata.data(i+1,1)... %[micron]
        rdata.data(i,1)...                        %[micron]
        ((rdata.data(i+1,1)+rdata.data(i,1))/2)...%[micron]
        (((rdata.data(i+1,1))^3 * pi *1/12) +...
        ((rdata.data(i,1))^3 * pi *1/12))];       %[micron^3]
    %% Number distribution
    PSD_data.n(k-i+1,1) = rdata.data(i,2)/...   %counted particles
        (rdata.data(i,1)-rdata.data(i+1,1))...  %/binwidth
        /rdata.data(k+3,1);                     %/measured volume
    %% Volume distribution=counted p* their volume/binwidth/measured volume
    PSD_data.v(k-i+1,1) = rdata.data(i,2)*PSD_data.bin(k-i+1,4)/...
        (rdata.data(i,1)-rdata.data(i+1,1))...
        /rdata.data(k+3,1);
    %% Total particle volume = bin volume * bin count/measured volume
    PSD_data.V = PSD_data.V +...
        PSD_data.bin(k-i+1,4) * rdata.data(i,2)/rdata.data(k+3,1);
end
%% Measured volume
PSD_data.v_m = rdata.data(k+3,1);                          %[cm^3]
%% Measured time
PSD_data.t_m = rdata.data(k+4,1);                          %[s]
%% Total particles concentration
PSD_data.C = sum(rdata.data(1:k,2))/rdata.data(k+3,1);     %[particles/cm^3]
                                                           %[micron^3/cm^3]
%% Date and time of measurement (Excel format!)
PSD_data.datetime = datestr(rdata.data(k+2) + datenum(1899,12,30));
```

diff_n.m

```
function [ dndt ] = diff_n(t, n )
%% derivative function of particle size distribution depending on
%% coagulation kernel.
%% n(1...I)  [particles/m^3] in each bin (discrete count)
global K_or Kr_aw t_end

% Kernel calculation
N = sum(n);
r=N^-(1/3);
```

```
K = K_or+ Kr_aw/r;
% pre-allocation
dndt = zeros(length(n),1);

%% Calculation loop
parfor i=1:length(n)  %%Multi-threaded if possible
    creation = 0;
    for j = 1:(i-1)
        creation = creation +...
            (0.5 * K(i-j,j) * n(j) * n(i-j));
    end

    destruction = 0;
    for j = 1:length(n)
        destruction = destruction + ...
            (n(i) * K(i,j) * n(j));
    end

    dndt(i,1) = creation - destruction;
end
waitbar(t/t_end)
end
```

References

1. González, I.A., J.A. Gallego-Juárez, and E. Riera, The influence of entrainment on acoustically induced interactions between aerosol particles—an experimental study. Journal of aerosol science, 2003. 34(12): p. 1611-1631.
2. Riera, E., J.A. Gallego-Juárez, and T.J. Mason, Airborne ultrasound for the precipitation of smokes and powders and the destruction of foams. Ultrasonics Sonochemistry, 2006. 13(2): p. 107-116.
3. Towler, G. and R. Sinnott, Chapter 18 - Specification and Design of Solids-Handling Equipment, in Chemical Engineering Design (Second Edition). 2013, Butterworth-Heinemann: Boston. p. 937-1046.
4. Khan, A.A., et al., Biomass combustion in fluidized bed boilers: Potential problems and remedies. Fuel Processing Technology, 2009. 90(1): p. 21-50.
5. Donaldson, K., et al., Ultrafine particles. Occupational and environmental medicine, 2001. 58(3): p. 211-216.
6. Heyder, J., et al., Deposition of particles in the human respiratory tract in the size range 0.005–15 mm. Journal of Aerosol Science, 1986. 17(5): p. 811-825.
7. Gallego Juárez, J.A., Macrosonics: Phenomena, transducers and applications. 2002.
8. Ferin, J., G. Oberdörster, and D. Penney, Pulmonary retention of ultrafine and fine particles in rats. American journal of respiratory cell and molecular biology, 1992. 6(5): p. 535.
9. Warheit, D.B., How meaningful are the results of nanotoxicity studies in the absence of adequate material characterization? Toxicological sciences, 2008. 101(2): p. 183-185.
10. Moradi, F., et al., Deactivation of oxidation and SCR catalysts used in flue gas cleaning by exposure to aerosols of high- and low melting point salts, potassium salts and zinc chloride. Applied Catalysis B: Environmental, 2003. 46(1): p. 65-76.
11. Zheng, Y., A.D. Jensen, and J.E. Johnsson, Deactivation of V2O5-WO3-TiO2 SCR catalyst at a biomass-fired combined heat and power plant. Applied Catalysis B: Environmental, 2005. 60(3–4): p. 253-264.
12. Mermelstein, J., M. Millan, and N.P. Brandon, The impact of carbon formation on Ni–YSZ anodes from biomass gasification model tars operating in dry conditions. Chemical Engineering Science, 2009. 64(3): p. 492-500.
13. Krasnyi, B.L., et al., Porous Permeable Ceramics for Filter Elements Cleaning Hot Gases from Dust. Glass and Ceramics, 2005. 62(5-6): p. 134-138.
14. de Jong, W., et al., Biomass and fossil fuel conversion by pressurised fluidised bed gasification using hot gas ceramic filters as gas cleaning. Biomass and Bioenergy, 2003. 25(1): p. 59-83.
15. Holdich, R.G., Fundamentals of Particle Technology. 2002: Midland Information Technology and Publishing.
16. Rhodes, M., Introduction to Particle Technology. 2008: Wiley.
17. Song, L., G. Koopman, and T. Hoffmann, An improved theoretical model of acoustic agglometation. Journal of vibration and acoustics, 1994. 116(2): p. 208-214.
18. Wilson, I.D., Encyclopedia of separation science. 2000: Academic Press.
19. Kundt, A., Ueber eine neue Art akustischer Staubfiguren und über die Anwendung derselben zur Bestimmung der Schallgeschwindigkeit in festen Körpern und Gasen. Annalen der Physik, 1866. 203(4): p. 497-523.
20. Wood, E. and A.L. Loomis, XXXVIII. The physical and biological effects of high-frequency sound-waves of great intensity. The London, Edinburgh, and Dublin Philosophical Magazine and Journal of Science, 1927. 4(22): p. 417-436.
21. Fuks, N.A., The mechanics of aerosols. 1964: Dover Publications.

22. MEDNIKOV, E.P., ACOUSTIC COAGULATION AND PRECIPITATION OF AEROSOLS. 1965.
23. DA C ANDRADE, E. AND S. LEWER, NEW PHENONEMA IN A SOUNDING DUST TUBE. NATURE, 1929. 124: P. 724-725.
24. PATTERSON, H. AND W. CAWOOD, PHENOMENA IN A SOUNDING TUBE. NATURE, 1931. 127(3920): P. 667-680.
25. GALLEGO-JUAREZ, J., G. RODRIGUEZ-CORRAL, AND L. GAETE-GARRETON, AN ULTRASONIC TRANSDUCER FOR HIGH POWER APPLICATIONS IN GASES. ULTRASONICS, 1978. 16(6): P. 267-271.
26. SCOTT, D., A NEW APPROACH TO THE ACOUSTIC CONDITIONING OF INDUSTRIAL AEROSOL EMISSIONS. JOURNAL OF SOUND AND VIBRATION, 1975. 43(4): P. 607-619.
27. SHAW, D. AND K. TU, ACOUSTIC PARTICLE AGGLOMERATION DUE TO HYDRODYNAMIC INTERACTION BETWEEN MONODISPERSE AEROSOLS. JOURNAL OF AEROSOL SCIENCE, 1979. 10(3): P. 317-328.
28. RIERA-FRANCO DE SARABIA, E. AND J. GALLEGO-JUAREZ, ULTRASONIC AGGLOMERATION OF MICRON AEROSOLS UNDER STANDING WAVE CONDITIONS. JOURNAL OF SOUND AND VIBRATION, 1986. 110(3): P. 413-427.
29. TIWARY, R. AND G. REETHOF, NUMERICAL SIMULATION OF ACOUSTIC AGGLOMERATION AND EXPERIMENTAL VERIFICATION. JOURNAL OF VIBRATION AND ACOUSTICS, 1987. 109(2): P. 185-191.
30. SOMERS, J., ET AL., ACOUSTIC AGGLOMERATION OF LIQUID AND SOLID AEROSOLS: A COMPARISON OF A GLYCOL FOG AND TITANIUM DIOXIDE. JOURNAL OF AEROSOL SCIENCE, 1991. 22: P. S109-S112.
31. GALLEGO-JUAREZ, J.A., ET AL., APPLICATION OF ACOUSTIC AGGLOMERATION TO REDUCE FINE PARTICLE EMISSIONS FROM COAL COMBUSTION PLANTS. ENVIRONMENTAL SCIENCE & TECHNOLOGY, 1999. 33(21): P. 3843-3849.
32. BUNTSMA, J., ACOUSTIC AGGLOMERATION AS A PRETREATMENT TO ENHANCE PARTICLE SEPARATION IN BIOMASS GASIFICATION HOT GAS CLEANUP, IN 3ME, PROCESS AND ENERGY TECHNOLOGY. 2012, TU DELFT: DELFT.
33. FINCH, R.D., INTRODUCTION TO ACOUSTICS. 2005: PEARSON/PRENTICE HALL.
34. KUNDU, P.K. AND I.M. COHEN, FLUID MECHANICS. 2010: ELSEVIER SCIENCE.
35. NIEUWSTADT, F.T.M., NOTES AND EXERCISES ACCOMPANYING THE LECTURE SERIES ADVANCED FLUID MECHANICS B56A. LAB. AERO- EN HYDRODYNAMICS, LEEGHWATERSTRAAT 21, 2628 CA DELFT.
36. OSEEN, C.W., ÜBER DIE STOKESSCHE FORMEL UND ÜBER EINE VERWANDTE AUFGABE IN DER HYDRODYNAMIK. ARK. MAT. ASTRON. FYS, 1910. 6(29): P. 1-20.
37. CHESTER, W., D. BREACH, AND I. PROUDMAN, ON THE FLOW PAST A SPHERE AT LOW REYNOLDS NUMBER. J. FLUID MECH, 1969. 37(04): P. 751.
38. TEMKIN, S., GASDYNAMIC AGGLOMERATION OF AEROSOLS. I. ACOUSTIC WAVES. PHYSICS OF FLUIDS, 1994. 6: P. 2294.
39. BRANDT, O., H. FREUND, AND E. HIEDEMANN, ZUR THEORIE DER AKUSTISCHEN KOAGULATION. KOLLOID-ZEITSCHRIFT, 1936. 77(1): P. 103-115.
40. DENISOV, A., A. PODOL'SKII, AND V. TURUBAROV, ENTRAINMENT OF AEROSOL PARTICLES IN AN ACOUSTIC FIELD AT REYNOLDS NUMBERS R. SOVIET PHYSICS: ACOUSTICS, 1965. 11(1): P. 92.
41. GONZALEZ-GOMEZ, I., T.L. HOFFMANN, AND J.A. GALLEGO-JUAREZ, THEORY AND CALCULATION OF SOUND INDUCED PARTICLE INTERACTIONS OF VISCOUS ORIGIN. ACTA ACUSTICA UNITED WITH ACUSTICA, 2000. 86(5): P. 784-797.
42. ANDRADE, E.D.C., THE COAGULATION OF SMOKE BY SUPERSONIC VIBRATIONS. TRANSACTIONS OF THE FARADAY SOCIETY, 1936. 32: P. 1111-1115.
43. HOFFMANN, T.L., AN EXTENDED KERNEL FOR ACOUSTIC AGGLOMERATION SIMULATION BASED ON THE ACOUSTIC WAKE EFFECT. JOURNAL OF AEROSOL SCIENCE, 1997. 28(6): P. 919-936.
44. TIMOSHENKO, V.I., AGGREGATION OF AEROSOL PARTICLES IN A SOUND FIELD UNDER THE CONDITIONS OF STOKES LAW FLOW. SOVIET PHYSICS-ACOUSTICS, 1965. 11(2): P. 183-186.
45. DONG, S., B. LIPKENS, AND T. CAMERON, THE EFFECTS OF ORTHOKINETIC COLLISION, ACOUSTIC WAKE, AND GRAVITY ON ACOUSTIC AGGLOMERATION OF POLYDISPERSE AEROSOLS. JOURNAL OF AEROSOL SCIENCE, 2006. 37(4): P. 540-553.

46. DIANOV, D., A. PODOLSKII, AND V. TURUBAROV, CALCULATION OF THE HYDRODYNAMIC INTERACTION OF AEROSOL PARTICLES IN A SOUND FIELD UNDER OSEEN FLOW CONDITIONS. SOV. PHYS. ACOUST, 1968. 13(3): P. 314-319.
47. SHENG, C. AND X. SHEN, MODELLING OF ACOUSTIC AGGLOMERATION PROCESSES USING THE DIRECT SIMULATION MONTE CARLO METHOD. JOURNAL OF AEROSOL SCIENCE, 2006. 37(1): P. 16-36.
48. CHENG, M., ET AL., ORTHOKINETIC AGGLOMERATION IN AN INTENSE ACOUSTIC FIELD. JOURNAL OF COLLOID AND INTERFACE SCIENCE, 1983. 91(1): P. 176-187.
49. SMOLUCHOWSKI, M.V., VERSUCH EINER MATHEMATISCHEN THEORIE DER KOAGULATIONSKINETIK KOLLOIDER LÖSUNGEN. Z. PHYS. CHEM, 1917. 92(129-168): P. 9.
50. EZEKOYE, O.A. AND Y.W. WIBOWO, SIMULATION OF ACOUSTIC AGGLOMERATION PROCESSES USING A SECTIONAL ALGORITHM. JOURNAL OF AEROSOL SCIENCE, 1999. 30(9): P. 1117-1138.
51. PHILIPS, PIEZOELECTRIC CERAMICS

PERMANENT MAGNET MATERIALS, IN DATA HANDBOOK COMPONENTS AND MATERIALS. 1982, PHILIPS: EINDHOVEN.

52. CHEN, Y.-C., LANGEVIN TYPE PIEZOELECTRIC TRANSDUCER WITH DIFFERENT MASS LOADING ON BOTH ENDS. DEPARTMENT OF ELECTRONICS ENGINEERING AND COMPUTER SCIENCE, TUNG-FANG INSTITUTE OF TECHNOLOGY.
53. CHACÓN, D., ET AL., A PROCEDURE FOR THE EFFICIENT SELECTION OF PIEZOELECTRIC CERAMICS CONSTITUTING HIGH-POWER ULTRASONIC TRANSDUCERS. ULTRASONICS, 2006. 44: P. E517-E521.
54. MORENO, E., ET AL. DESIGN AND CONSTRUCTION OF A BOLT-CLAMPED LANGEVIN TRANSDUCER. IN ELECTRICAL AND ELECTRONICS ENGINEERING, 2005 2ND INTERNATIONAL CONFERENCE ON. 2005. IEEE.
55. IULA, A., ET AL., FINITE ELEMENT THREE-DIMENSIONAL ANALYSIS OF THE VIBRATIONAL BEHAVIOUR OF THE LANGEVIN-TYPE TRANSDUCER. ULTRASONICS, 2002. 40(1): P. 513-517.
56. YAO, Q. AND L. BJORNO, BROADBAND TONPILZ UNDERWATER ACOUSTIC TRANSDUCERS BASED ON MULTIMODE OPTIMIZATION. ULTRASONICS, FERROELECTRICS AND FREQUENCY CONTROL, IEEE TRANSACTIONS ON, 1997. 44(5): P. 1060-1066.
57. MULTIPHYSICS, C. 2012.
58. LECTURE NOTES ON MULTIPHYSICS FROM THE TECHNICAL UNIVERSITY OF MONTANA.
59. MERKUS, H.G., PARTICLE SIZE MEASUREMENTS: FUNDAMENTALS, PRACTICE, QUALITY. VOL. 17. 2009: SPRINGER.
60. MERCER, T.T., M.I. TILLERY, AND G.J. NEWTON, A MULTI-STAGE, LOW FLOW RATE CASCADE IMPACTOR. JOURNAL OF AEROSOL SCIENCE, 1970. 1(1): P. 9-15.
61. BEMER, D., J.F. FABRIES, AND A. RENOUX, CALCULATION OF THE THEORETICAL RESPONSE OF AN OPTICAL PARTICLE COUNTER AND ITS PRACTICAL USEFULNESS. JOURNAL OF AEROSOL SCIENCE, 1990. 21(5): P. 689-700.
62. PANDIS, S.N., ET AL., INVERSION OF AEROSOL DATA FROM THE EPIPHANIOMETER. JOURNAL OF AEROSOL SCIENCE, 1991. 22(4): P. 417-428.
63. TOPAS, LASER AEROSOL PARTICLE SIZE SPECTROMETER LAP320 INSTRUCTION MANUAL.
64. GEBHART, J., RESPONSE OF SINGLE-PARTICLE OPTICAL COUNTERS TO PARTICLES OF IRREGULAR SHAPE. PARTICLE & PARTICLE SYSTEMS CHARACTERIZATION, 1991. 8(1-4): P. 40-47.
65. CARTER, W. AND I. HASEGAWA, FIXATION OF TOBACCO SMOKE AEROSOLS FOR SIZE DISTRIBUTION STUDIES. JOURNAL OF COLLOID AND INTERFACE SCIENCE, 1975. 53(1): P. 134-141.
66. KEITH, C., PARTICLE SIZE STUDIES ON TOBACCO SMOKE. BEITRAGE ZUR TABAKFORSCHUNG INTERNATIONAL, 1982. 11: P. 123.
67. MOLINE, J.M., ET AL., HEALTH EFFECTS EVALUATION OF THEATRICAL SMOKE, HAZE, AND PYROTECHNICS. EQUITY-LEAGUE PENSION AND HEALTH TRUST FUNDS, 2000.
68. RADACSI, N., ET AL., ELECTROSPRAY CRYSTALLIZATION FOR HIGH-QUALITY SUBMICRON-SIZED CRYSTALS. CHEMICAL ENGINEERING & TECHNOLOGY, 2011. 34(4): P. 624-630.
69. SCHWYN, S., E. GARWIN, AND A. SCHMIDT-OTT, AEROSOL GENERATION BY SPARK DISCHARGE. JOURNAL OF AEROSOL SCIENCE, 1988. 19(5): P. 639-642.

70. YANG, T.-T., ET AL., CHARACTERIZATION OF POLYCYCLIC AROMATIC HYDROCARBON EMISSIONS IN THE PARTICULATE PHASE FROM BURNING INCENSES WITH VARIOUS ATOMIC HYDROGEN/CARBON RATIOS. SCIENCE OF THE TOTAL ENVIRONMENT, 2012. 414: P. 335-342.
71. YANG, C.-R., T.-C. LIN, AND F.-H. CHANG, PARTICLE SIZE DISTRIBUTION AND PAH CONCENTRATIONS OF INCENSE SMOKE IN A COMBUSTION CHAMBER. ENVIRONMENTAL POLLUTION, 2007. 145(2): P. 606-615.
72. GALLEGO-JUÁREZ, J.A., ET AL., A MACROSONIC SYSTEM FOR INDUSTRIAL PROCESSING. ULTRASONICS, 2000. 38(1): P. 331-336.
73. LEHTINEN, K.E., THEORETICAL STUDIES ON AEROSOL AGGLOMERATION PROCESSES. 1997: TECHNICAL RESEARCH CENTRE OF FINLAND.
74. BRANDT, E., LEVITATION IN PHYSICS. SCIENCE, 1989. 243(4889): P. 349-355.
75. WHYMARK, R., ACOUSTIC FIELD POSITIONING FOR CONTAINERLESS PROCESSING. ULTRASONICS, 1975. 13(6): P. 251-261.
76. GALLEGO-JUÁREZ, J., ET AL., POWER ULTRASONIC TRANSDUCERS WITH EXTENSIVE RADIATORS FOR INDUSTRIAL PROCESSING. ULTRASONICS SONOCHEMISTRY, 2010. 17(6): P. 953-964.
77. KÖNIG, W., HYDRODYNAMISCH-AKUSTISCHE UNTERSUCHUNGEN. ANNALEN DER PHYSIK, 1891. 278(3): P. 353-370.
78. TEMKIN, S. AND S. TEMKIN, ELEMENTS OF ACOUSTICS. 1981: WILEY NEW YORK.